# The Effects of Grain Size on Dislocations organization and Internal Stresses developed under Tensile Loading in f.c.c. metals

Xavier Feaugas, Haddou Hakim


# The Effects of Grain Size on Dislocations organization and Internal Stresses developed under Tensile Loading in f.c.c. metals

| | |
|---|---|
| Journal: | *Philosophical Magazine & Philosophical Magazine Letters* |
| Manuscript ID: | TPHM-06-Apr-0093.R2 |
| Journal Selection: | Philosophical Magazine |
| Date Submitted by the Author: | 07-Sep-2006 |
| Complete List of Authors: | Feaugas, Xavier; Université de La Rochelle, LEMMA<br>Hakim, Haddou; UTC |
| Keywords: | dislocation structures, grain size, mechanical behaviour, nickel, polycrystalline metals, stainless steels, statistical physics |
| Keywords (user supplied): | |

# The Effects of Grain Size on Dislocations organization and Internal Stresses developed under Tensile Loading in f.c.c. metals

X. FEAUGAS[1] AND H. HADDOU[2]

(1) LEMMA, EA3167, Université de La Rochelle, 25 av. Enrico Fermi - 17000 La Rochelle, France.
(2) Laboratoire Roberval, UMR CNRS 6066, UTC, BP 20529 – 60205 Compiègne cedex, France.



The relation between deformation and dislocation properties has been studied for pure polycrystalline nickel and austenitic stainless steel AISI 316L in stage III. Special care was taken to study statistically the effects of the grain size and grain orientation on dislocations densities and distribution. It is shown that the nature of dislocations cells depends on the grain size and crystallographic orientation. The dimensional parameters which depend on the grain size, i.e. the inter-boundary spacing (λ) and the boundary thickness (e) define three domains of crystallographic orientation and depend on the grain size. Scaling hypotheses reveal two physical mechanisms which, at this level of plastic strain, are correlated to a specific value of the noise, associated with the distribution functions. A similitude between structural parameters and dislocation densities in each phase (walls and inter-walls spacing) is identified and discussed in terms of kinetic equations describing dislocation density evolutions and of fluctuations of certain physical parameters. This similitude provides a physical signification of the scaling distribution obtained on λ and e in terms of a stochastic approach of dislocation distribution. The origin of Hall-Petch behaviour observed at large strain is interpreted in terms of an interaction between inter-granular and intra-granular long-range internal stresses, which depends on the grain size. We conclude that, at high strain, the Hall & Petch phenomenological relation is a consequence of plastic strain history and of strain gradient in grains. From this last point naturally arises a length scale which depends on stacking fault energy.

*Keywords*: Dislocation pattern, grain size, scaling behaviour, long-range internal stresses

## 1. Introduction

The influence of grain size (d) on strength hardening in metals and alloys has received considerable interest for several decades. The empirical Hall-Petch relation ($\sigma = \sigma_0 + k_0 \times d^{-1/2}$, d is the mean grain diameter, $\sigma_0$ and $k_0$ are constants at a particular plastic strain) has been currently used to describe the relationship between yield strength and grain size of metals. Whereas physical models [1-8] correctly predict the Hall-Petch relation, the origin of this behaviour still remains actively debated [9-23]. As a whole, these models are focused on low strain and either fail to show the flow stress dependence on grain at higher plastic strain or predict a relation other than that proposed by Hall and Petch. In fact, the validity of the Hall-Petch relation at large plastic strain has been clearly established experimentally [24-28]. In this case though, the strain dependence of the factor $k_0$ differs from one work-hardening stage to the next. $k_0$ increases with strain in stage I and then decreases in stages II and III. The transition between increasing and decreasing parts has been recently correlated with the heterogeneous distribution of dislocation in grains. Based on a flow stress partition in terms of short and long-range internal stresses, the origin of the Hall-Petch relationship at the different levels of microstructure heterogeneities has been clarified [28]. The grain size effect on the short-range stresses (the effective stresses) is well explained in terms of a mean free path associated with mesh size in the grain boundary. In stage I, the long-range internal stresses dependence on grain size appears to result mainly from inter-granular plastic-strain incompatibilities associated with the formation of a layer near grain-boundary [7, 29]. At high plastic strain, the decrease in the dependence of long-range internal stresses on grain size is understood as an increase in intra-granular long-range internal stresses and a decrease in inter-granular long-range internal stresses. However, the crucial assumption that intra-granular long-range internal stresses do not depend on grain size has been seriously questioned [23]. Indeed, it has been recently suggested that the fact that the average cell size $\langle\lambda\rangle$ does not depend on grain size in stage III (Figure 1) is not sufficient to validate the previous assumption. Moreover, $\langle\lambda\rangle$ is an increasing function of the grain size at given plastic strain in stage II [30-32]. This observation is interpreted via the formation of dislocation cells at high stress with increasing grain size [28]. To sum up, the intra-granular internal stress seems to depend on grain size too. For this dependence to be evaluated quantitatively, however, one needs statistical studies of dislocation patterns as a function of grain size and grain orientation. While the latter has been explored by many authors in recent works on tensile [33-43] and cyclic [44-48] loadings, the former remains poorly documented [39]. In many f.c.c. alloys, dislocation patterning depends on the grain orientation with respect to the stress axis. Three kinds of dislocation walls are commonly reported: the geometrically necessary boundaries (GNBs), the incidental dislocation boundaries (IDBs) and the dipolar walls (DWs). The main part of the statistical analyses performed on boundary spacing has been devoted to GNBs [49-58], while fewer results have been proposed so far for IDBs [53, 54], despite the fact that the latter represent the main part of trapped dislocations at stages II and III. Under tensile loading, one expects the IDBs to contribute much more to intra-granular long-range internal stresses than GNBs in stage III. Investigating the effects of inter and intra-granular long-range internal stresses is part of the current debate on the kind of length scale one should take into account to describe strength hardening. In the present paper, we have investigated dislocation patterning as a function of grain orientation, grain size and stacking fault energy. As theoretical studies previously demonstrated (see [59]), statistical analyses provide a good approach of the physical parameters governing the hardening rate.

[insert Figure 1 about here]

## 2. Experimental procedure

An extending mechanical database of strength hardening of polycrystalline nickel and austenitic AISI 316L can be found in previous publications [28, 60]. In the present work, axi-symmetric smooth specimens were strengthened in tension only to discuss the interactions between strength hardening, dislocation distributions and grain size. Cylindrical specimens with 8 mm diameters and 10 mm gage lengths were cut from cold-dawn rods and recrystallized to a mean grain size range of 13 and 168 µm. Four and fives grain sizes have been studied respectively in nickel and AISI 316L. Thermal histories produced relatively week crystallographic texture [28, 60, 61] and a dislocation density below $10^{10}$ $m^{-2}$ [28, 30]. The tensile specimens were deformed to a predetermined plastic strain levels ($\varepsilon_p$) corresponding to the "conventional" stage III of strain hardening ($\varepsilon_p$= 30% for Ni and $\varepsilon_p$ =34% for AISI 316L). The dislocation microstructures (densities and distribution of dislocations) of individual grain were investigated using Transmission Electron Microscopy (TEM). These investigations were conducted using a Jeol JEM 2011 electron microscope operating at 200 kV on specimens cut parallel and perpendicular to stress axis. Foils for TEM were thinned in double twin-jet electro-polisher using electrolytes and conditions previously described [48, 60-62]. For each condition (plastic strain, material and grain size), densities and distributions of the dislocations were determined over 50 grains. Stereographic analysis (stereographic projection) was performed in each grain observed. Special care was taken in the marking of the TEM specimens so that the direction of the stress axis could be identified on stereographic map of each grain studied. The dislocation densities was determined from TEM micrographs by counting the number of intersection (N) between dislocations and a set of random test lines from foil areas of 0.1-0.25 $\mu m^2$ and by measuring the foil thickness (t). The estimation of local foil thickness (t) could be obtained with free dislocation line using stereographic project and different diffraction conditions (for more details see references [63, 64]).

## 3. Dislocations features

The effect of grain size and grain orientation on deformation microstructure was examined by TEM observations at stage III on two f.c.c. metals which presented a low stacking fault energy (AISI 316L, $\gamma_{SFE}/\mu b = 1.2\times10^{-3}$, $\gamma_{SFE}$ is the stacking fault energy, $\mu$ is the shear modulus and b is the burgers vector) and a high stacking fault energy (Ni, $\gamma_{SFE}/\mu b = 6.3\times10^{-3}$). A detailed analysis of the dislocation distribution (cells morphology, the size of cells ($\lambda$) and walls (e)) was conducted on each grain from nickel and austenitic stainless steel AISI 316L in specimens having different grain sizes. Irrespective of material studied and grain size, two aspects were investigated: a qualitative aspect related to the type of dislocation structures identified and a quantitative aspect (statistical analysis) in relation to dislocation density and distribution (size of cells and walls). The main part of the statistical measurement (50 measures in each grain) was conducted on nickel for two grain sizes (18 µm and 168 µm). The investigations on stainless steel are only associated with cells morphologies and dislocations densities in each grain in terms of mean values in a more restraint number of measures (near 10 by grain).

[insert Figure 2 about here]

### 3.1. *Qualitative observations*

As extensively demonstrated in the past [31, 32, 34, 36-38, 62, 65-76] the main dislocation feature observed in stage III is the cell structure. The microstructural observations (Figure 2)

show that the dislocation pattern within a grain is basically homogeneous but is observed to vary from grain to grain. In accordance with previous works on copper [37, 38] and aluminum [34, 36] dislocation distributions can be divided into three types as shown in Figure 2:

- Type I microstructure (Figure 2a) is subdivided in block by extending dislocations boundaries fairly straight and parallel to the most stressed slip plane $(\bar{1}11)$. According to previous works on f.c.c. alloys, a microstructure is defined as type I only if the average deviation of boundaries planes from the trace of {111} plane is lower than 5° [36]. Difference of contrast between two blocks (strong black-white contrast) is an illustration of lattice rotation induced by such dislocation configuration. Those boundaries are called geometrically necessary boundaries (GNBs) due to their accommodation of different crystal orientation changes on each side of a boundary [52]. These kite planar boundaries can probably result in the formation of grid structure in relation to the activation of two coplanar slip systems in the early stages of plastic strain [62]. This kind of wall has been well characterized at the transition between stage I and stage II from medium and low stacking fault energy alloys [62 65, 69, 77]. Their formations depend on the grain orientation, in accordance with slip activity as related in austenitic stainless steel [40, 76]. For large strains, the boundaries have been analyzed in aluminum: they showed that the boundaries following a slip plane have a mixed tilt and twist character [35, 56, 78, 79] in accordance with a deviation of hexagonal network [62] or with Franck's formula [80]. All these observations support the idea that GNBs formation occurs at the early stage of plastic strain. TEM observations suggest that walls stability for higher strain is probably linked to the formation of different kind of nodes like Lomer lock configuration [62, 80]. Quite equiaxed cells are observed between two GNBs. The boundaries of equiaxed cells, namely incidental dislocation boundaries (IDBs), are formed by trapping of glide dislocations arising due to the activation of more than one slip systems. The dislocation organization is bad in these walls. The mean value of dislocation densities in these walls $<\rho_w>$ is equal to $9\times10^{14}$ $m^{-2}$ irrespective of the grain size considered in nickel.

- Type II microstructure, namely equiaxed cell structure (Figure 2b) is subdivided by "ordinary" dislocation boundaries (IDBs). These boundaries differ from the GNBs observed in type I structures in that they show smaller misorientations across the boundaries (poor difference of contrast between cells). The mean value of dislocation densities in the walls ($<\rho_w>=9\times10^{14}$ $m^{-2}$) is similar to the one obtained for the IDBs observed between GNBs of type I microstructure. Grains with the tensile axis in the vicinity of [001] do not form extended planar boundaries which present a correlation to a slip plane because of a high degree of multiple slips (height equivalent slips).

- Type III microstructure is quite similar to the one observed in type I microstructure. Figure 2c shows extending dislocations boundaries less straight than type I boundaries which present a deviation larger than 5° from any slip planes. Then the microstructure is subdivided by "non-crystallographic" boundaries in accordance with a deviation of boundary plane from primary, conjugate and cross slips planes [41]. This last term can be moderated by the fact that some boundaries traces are parallel to a {001} plane in accordance with occurrence of Lomer locks [62]. The boundaries observed are not as easily defined as GNBs or IDBs because of a wavy morphology and a difference of contrast between two long-cells. The mean value of dislocation densities in the walls is higher than those measured for IDBs in the type I and type II microstructures ($<\rho_w>= 10^{15}$ $m^{-2}$). A quite similar result has been reported in copper [34].

[insert Figure 3 about here]

The occurrence of one microstructure depends on grain orientation and grain size from nickel (Figure 3). In higher grain size, a good correspondence between grain orientation and microstructural type is observed (Figure 3a). The observed microstructure types in nickel with grain size equal to 168 µm show similarity to those identified in the tensile strained aluminum [34, 36], copper [37, 38] and austenitic stainless steel [76], although there are some differences in the division pattern of the standard triangle (Figures 3a and 3b and see also Figure 4 in reference [34] and Figure 1 in reference [37]). The boundary lines separating the three types of structures in the standard stereographic triangle depend on the material studied. Consequently, the fraction of grain presenting one structure depends on stacking fault energy. Surprisingly, in low grain size (18 µm), only equiaxed cells (type II microstructure) are found irrespective of the orientation of grains (Figures 3c). In other words, the cell morphology seems to be depending on the grain size. The proportion of grains presenting types I and III cells ("elongated" cells) has been reported as a function of grain size in nickel and AISI 316L (Figure 4). For a grain size lower than a critical value ($d_c$), the elongated cells are not observed. This critical value depends on stacking fault energy: $d_c$ is higher in austenitic stainless steel AISI 316L than in nickel. Additionally, the proportion of grains presenting equiaxed cell structure is equal to 20% for a grain size higher than $d_c$ (80% of elongated cells). This last value does not seem to depend on the material studied and consequently not on stacking fault energy (Figure 4). These results are in contradiction with a study conducted on polycrystalline copper [39] where three microstructural dislocation patterns seem to be observed for a grain size of 3.8 µm. However, in this publication [39], the texture, the distribution of grain size and the initial dislocation density are either not specified or poorly documented ; it is thus impossible to discuss in the present work the origin of the difference between these two works. Specific texture, and strain history are possibilities which can be explored in further works.

[insert Figure 4 about here]

### 3.2. *Statistical analysis of morphological parameters*

For the microstructures in nickel and 316L deformed in tension in stage III, the microstructural parameters have been determined. These parameters are the spacing between walls ($\lambda$) and the wall thickness (e). In spite of the fact that the main part of this work is devoted to incidental dislocation boundaries, some results on geometrically necessary boundaries have been collected on nickel. The average GNBs spacing obtained in nickel (grain size equal to 168 µm) is equal to 0.8 µm for a plastic strain of 34%. For similar plastic strain (Von Mises plastic strain), this value is lower than the one reported in aluminum: ~3 µm [35, 57] and quite similar to the one obtained in nickel deformed in cold rolling ~0.99 µm [53]. Based on the fact that the wall thickness of GNB (0.04 µm) is lower than the one of IDB (~ 0.1 µm), the contribution of GNBs to the mean value of intra-granular internal stress in one grain has not been considered in the present work (the fraction of hard phase $f_w=e/e+\lambda$ is lower for GNB (~2.8 %) than for IDB (~20%), see Eq. 8 for more details) and we focused only on the IDBs boundaries. Independently of the type of heterogeneous dislocation distribution, the incidental dislocation boundaries (IDBs) are observed, for equiaxed cells (type II), for equiaxed cells between two GNB boundaries (type I) and for long cells (type III). A statistical analysis of these kinds of walls has been performed in terms of wall thickness (e), inter-wall spacing ($\lambda$) and dislocation density in walls ($\rho_w$) and in channel ($\rho_s$) (Figure 5). This analysis has been performed for two grain sizes in polycrystalline nickel strained in stage III.

[insert Figure 5 about here]

**3.2.1 – Dimensional parameters of cells**. According to the former works on the subject in f.c.c. alloys (generally performed for strains higher than the one imposed in the present work) fixed areas in each grain are scanned and (e, λ) measured on 50 cells. For each grain an average value <e> and <λ> has been calculated from the measured data. P(λ, λ+Δλ) and P(e, e+Δe) are defined as being the probabilities for any given boundary spacing and wall thickness to have a size between λ and λ+Δλ, and e and e+Δe respectively. To create histograms of probability, bindwidths have been chosen to be approximately Δλ=<λ>/3 and Δe=<e>/3. Figures 6 and 7 show some measured spacing distributions for different grain orientations and for grain sizes equal to 18 µm and 168 µm respectively. Similar results concerning size distribution of wall thickness are presented on Figures 8 and 9.

[insert Figures 6 and 7 about here]

*Boundaries spacing*. For low grain size, irrespective of grain orientation, mean spacing <λ> does not seem to be a determining value (Figure 6). For a high grain size, no correlation seems to be observed between <λ> and the type of cells or the grain orientation (Figure 7). Whatever the criterion used (the grain orientation and/or grain size) the probability distribution does not coincide. A scaling hypothesis has been applied in many situations (grain sizes [80], boundary misorientation angles [49-51, 53, 54, 58, 82], boundary spacings [52-54, 57, 58]) to provide an organizing principle. A similar approach is applied in the present work, in which the probability density functions normalized by the average spacing <λ>P(λ, λ+Δλ) are plotted against λ/<λ> in Figure 10a. In this figure, where only some grain studies are shown, the curves from different grain orientation collapse onto one curve. Thus the scaling hypothesis is verified in the first approach for type II microstructure and grain size equal to 18 µm. A systematic investigation of scaling hypothesis has been then performed for all the grains studies, using a distribution function f(x). The morphology of the distributions is asymmetric, which suggests that a reasonable description of them can be obtained by an empiric law like gamma distribution. The scaled distribution can be well described by the following function (Figure 10a):

$$f(x) = \frac{1}{\Gamma(\alpha+1)\beta^{\alpha+1}} x^{\alpha} \exp\left[\frac{-x}{\beta}\right] \text{ with } x=\lambda/\langle\lambda\rangle \qquad (1)$$

where α and β are fit parameters and Γ(α+1) is the gamma function. The mean value of x is given by <x>=β×(α+1) and the variance is $\sigma_\lambda^2=\beta^2\times(\alpha+1)$. In the present case <x> equals 1 by definition, and consequently $\beta=1/(\alpha+1)=\sigma_\lambda^2$. Thus the distribution function f(x) is defined for each grain using only two parameters <λ> and $\sigma_\lambda$. Considering all the grains studied, Figure 11a clearly shows that $\sigma_\lambda^2$ is a constant (0.08±0.02) which does not depend on the mean value of boundary spacing, <λ>. Moreover, $\sigma_\lambda^2$ seems not to be affected by grain orientation, grain size and the type of microstructure developed. Consequently, all the distributions collapse into a single distribution when scaled by the average boundary spacings. Furthermore, <λ> is a function of the grain size and grain orientation (Figures 12a and 12c). For a grain size equal to 168 µm (Figure 12c), the IDBs boundaries spacing <λ> depends on the type of microstructure with the following ascending order: $\langle\lambda\rangle_{(\text{type II})} > \langle\lambda\rangle_{(\text{type III})} > \langle\lambda\rangle_{(\text{type I})}$ . Despite the fact that only one type of microstructure is observed for a grain size equal to 18 µm, Figure 12a points out the fact that three domains can be defined on stereographic triangle. These domains are

similar to the ones observed in terms of microstructure for higher grain size (d= 168 µm, Figures 3a and 12c). Basing ourselves on these observations, we can conclude that the grain orientation does not affect the type of microstructure in low grain sizes but modifies the dimensional parameter which characterizes this microstructure (equiaxed cell).

[insert Figures 8 and 9 about here]

*Wall thickness*. In the same way as for boundary spacings, the mean value and the probability distribution of wall thickness depend on grain orientation irrespective of the grain size (Figures 8 and 9). A scaling hypothesis has been applied to provide an organizing principle. The probability density functions normalized by the average thickness $\langle e \rangle P(e, e+\Delta e)$ were plotted against $e/\langle e \rangle$ in Figure 10b. In this figure, where only some grains studied were shown, the curves from different grain orientations collapse onto one curve. Thus the scaling hypothesis is verified in the first approach for type II microstructure and a grain size equal to 168 µm. A systematic investigation of scaling hypothesis was then performed for all the grains studies, using a distribution function f(x) (eq. 1) with $x=e/\langle e \rangle$. The distribution function f(x) is defined for each grain using only two parameters $\langle e \rangle$ and $\sigma_e$. Figure 11b shows the evolution of $\sigma_e^2$ as a function of $\langle e \rangle$. Two domains can be clearly established : $\sigma_e^2$ decreases as a function of $\langle e \rangle$ under a threshold mean thickness equal to 80 nm, then $\sigma_e^2$ stays constant and equals 0.08±0.02 for values of $\langle e \rangle$ higher than the threshold. This result does not depend on the type of dislocation structures, crystallographic orientation, and grain size. For $\langle e \rangle$ higher than 80 nm, all the distributions collapse into a single distribution when scaled by the average boundary spacing. However, the evolution of $\sigma_e^2$ as a function of $\langle e \rangle$ for $\langle e \rangle$ lower than 80 nm can probably be correlated with a progressive transformation of IDB to GNB when $\langle e \rangle$ decreases during stage III [62]. Further results, $\langle e \rangle$ is a function of the grain size and grain orientation (Figures 12b and 12d). For a grain size equal to 168 µm (Figure 12d) the thickness $\langle e \rangle$ of IDBs boundaries depends on the type of microstructure with a following ascending order $\langle e \rangle_{(\text{type III})} > \langle e \rangle_{(\text{type I})} > \langle e \rangle_{(\text{type II})}$. This sequence is different from the one obtained for the boundaries spacing $\langle \lambda \rangle$. In spite of the fact that only one type of microstructure is observed for a grain size of 18 µm, Figure 12b points out the fact that three domains can be defined on stereographic triangle in terms of wall thickness (e). These domains are similar to the ones observed in terms of microstructure for higher grain sizes (d= 168 µm, Figures 3a and 12d). Based on these observations, in the same way as boundary spacing, grain orientation does not affect the type of microstructure in low grain sizes but it modifies the dimensional parameter $\langle e \rangle$ which characterizes the microstructure (equiaxed cell). We can sum up these observations by saying that intra-granular heterogeneity (dislocations distribution) is dependent on the grain size and on the grain orientation, regardless of the range of grain size considered.

[insert Figures 10,11 and 12 about here]

**3.2.2. Relation between dislocation densities, cell size and wall size**. In order to approach the intra-granular internal stresses, we were brought to make systematic measurements of the dislocation densities. The measurements were made in « hard phase » ($\rho_w$, w for « walls ») and in « soft phase » ($\rho_s$). The aim was to correlate the thickness of wall (e) to the dislocation density ($\rho_w$) as well as the size of the cells ($\lambda$) to the density in the soft zones ($\rho_s$). These correlations were made using our own measures in the case of the nickel (Figure 13a) and starting from work of Gaudin [43] for the 316L (Figure 13b). A relation was clearly established between the geometrical parameters of the cells and the densities of dislocations.

Thus, it was noted that the parameters λ and e were inversely proportional to the square root of the dislocation density $\rho_s$ and $\rho_w$ respectively:

$$e = A \cdot \rho_w^{-0.5} \text{ and } \lambda = B \cdot \rho_s^{-0.5} \quad (2)$$

These equations are in accordance with the experimental data for both materials. Moreover, it seems that A is equal to B in the two materials studied. Consequently, a structure of dislocation will be characterized only by two structural parameters (e, λ) or ($\rho_s$, $\rho_w$). This kind of relation does not depend on the crystallographic orientation and the size of the grains considered, but seems to be only a function of the nature of material. (e, λ) are less dependent on ($\rho_s$, $\rho_w$) in austenitic stainless steel (A=B=2) than in nickel (A=B=4) and the one reported by Mughrabi in copper (A=4±15%) [83]. Consequently, A depends on stacking fault energy and seems to be lower when $\gamma_{sfe}/\mu b$ is low as well.

[insert Figure 13 about here]

## 4. Discussion

Strain hardening results from various forms of intersecting dislocations and storage of glide dislocations during strengthening. The storage of dislocation is due to a continuous production of "sessile" dislocation configuration (locks, jogs, debris, cross-slipped segments …), obstacles with shearing strain that anchor the captured mobile dislocations into bundles or boundaries [84]. The numerical [85] and experimental [62, 86, 87] studies confirm that cross-slip strongly favours the emergence of ordered dislocation structures through, for example, a progressive transformation of pile-up to a dipoles and multipoles bundle. However, it is not the only possibility explaining the phenomenon of patterning. Recently, many experimental works [34, 36-38, 41, 42, 88] supported the idea that heterogeneous dislocation distribution depended on slip activity. Studying the cells morphologies obtained in stage III as a function of grain size and stacking fault energy can elucidate some parts of this debate.

### *4.1. Microstructures morphology*

The dislocation pattern within a grain is basically homogeneous in stage III, which is not the case for low plastic strain i.e. stages I and II, where a gradient of strain is related near grain boundaries [28, 89, 90]. An expression of this gradient is characterized by a dislocation density which evolves between the vicinity of the grain boundary ($\rho_{VGB}$) and the grain interior (ρ). The difference between the two dislocation densities decreases as a function of plastic strain to reach a value near zero at a plastic strain which depends on stacking fault energy and grain size [28, 89]. This threshold strain increases with the increase in the grain size and $\gamma_{SFE}$ respectively. These results are consistent with the present results which demonstrate an homogenization of plastic strain in grain at stage III at a plastic strain near 30%. However, we cannot conclude that inter-granular long-range internal stresses are suppressed, as suggested in previous works [28, 62, 92]. The partial or complete reduction of elastic and plastic strain incompatibilities between grains remains an open question which can be discussed using a statistical approach (see § 4.4).

The first extensive results about the effect of stress axis on dislocation microstructure have been reported by Kawasaki [70-72] in copper single crystals with different crystallographic directions parallel to tensile direction. The correlation between the grain orientation and the crystallographic boundary planes shows that the boundary orientation is linked to the active slip systems. An interesting review of these aspects has been given by Liu and Hansen [33].

Recently, Winter *et al.* demonstrated that this observation could be explained by a Schmid factor analysis assuming activity on the five most stressed slip systems [41, 42]. One would therefore expect that the morphology of dislocation patterning results in slip activity more than in grain orientation. This fact can be well demonstrated in terms of grain size influence on stress-strain state in grain. The slip pattern depends on the grain orientation with respect to the deformation axes but also on stress-strain interactions between neighbouring grains. The role of inter-granular long-range internal stresses on the activation of multiple slip has been often reported in polycrystalline approaches of metal plasticity (see [91]); it was also suggested [41] by comparing the grain boundaries developed in grains and in monocrystals strengthening in the same direction. The main difference observed between those two samples is obtained for orientations generally favourable for primary slip. In the present work, the decrease in grain size enhances inter-granular long-range internal stresses [28] which promote multiple slip in the early stages of plastic strain [93-96] and consequently the simultaneous activation of a number of slip systems higher than the one predicted by a Schmid factor analysis. In other words, a small grain size favours a stress state in grain which allows the activation of a number of slips near the one obtained in monocrystal strengthening in [001] direction. Then it is not surprising to observe only equiaxed cells (type II) for the lower grain sizes ($d<d_c$) in nickel and austenitic stainless steel. Quite similar results have been recently observed under multiaxial cyclic loadings, where equiaxed cells formation is associated with multiple slips induced by non-proportional loadings [97, 98]. In accordance with recent analyses of the evolution of the lattice plane misorientation during deformation, it can be concluded that IDBs are promoted by multiple slip deformation contrary to GNBs which are the result of a less deviation of single-slip deformation [132]. The effect of stacking fault energy on the threshold grain size $d_c$ can be elucidated in terms of cross slip activity. A decrease of $\gamma_{SFE}$ reduces cross-slip activity and consequently increases the activation of multiple slips to reduce plastic strain incompatibilities between grains. Consequently, the formation of equiaxed cells in all the grain orientations is observed in a grain size range higher in 316L (low SFE) than in nickel (high SFE) : $d_c(Ni)<d_c(316L)$. For large grain sizes however, the existence of a boundary dependence on the grain orientation shows that grain interactions are of minor importance. Consequently, in a qualitative point of view, inter-granular long range internal stresses clearly affect the intra-granular stress-strain state and the dislocation distribution in grains at large strain (~30%).

### *4.2. Similitude between structural parameters and dislocation densities*

Dislocation patterning is a self-organization process which occurs during strengthening of metals under different kinds of loading conditions. The contribution of a heterogeneous dislocation distribution on work hardening is at the present time the subject of many discussions. As mentioned by Argon [84] and by Nabarro [99], plastic strain evolution in f.c.c. metals is made up of different sequences of dislocations patterns. This fact has been documented for the first time long ago by Steeds in copper single crystals [65]. Consequently, two central questions arise from this last comment: firstly, how can interactions of clustered dislocations with mobile ones affect work hardening? And secondly, in one sequence of strengthening, why only certain patterns are formed and stay stable? The last question is a relevant challenge of dislocation theory which has motivated several approaches [59, 101-109]. The first group of models is based on the assumption that dislocation distribution arises from a principle of minimization of elastic energy [103]. This thermodynamic approach has been criticized because it can be applied only to an equilibrium system, which is not the case under loading. An alternative to these models is a statistical approach of the different fluctuations of the physical parameters which characterize or interact with plastic strain (dislocation velocity, densities, interactions, internal stresses..). These models have in

common the fact that they provide a possible explanation for the experimentally [66] established scaling relation between cell size λ and the average dislocation spacing ($\sim\rho^{-1/2}$). It seems now well established that this relation depends on a correlation between dislocation glide [104], kinematics aspect of patterning [83, 106]) and/or a minimization of elastic stored energy [103]. An interesting point exposed by Mughrabi [83] is the fact that this relation results in a specific behaviour in a quasi-steady state of each "phase" in a composite description of dislocation pattern. Following an original paper of Essmann and Mughrabi [110], the kinetic equation which takes the rate production and rate annihilation of dislocations into account can be established as follows:

$$d\rho_i = \frac{k_i}{bd_i} d\gamma_i - 2\frac{y_i}{b}\rho_i P d\gamma_i \text{ with } i \in \{c, w\} \quad (3)$$

where $d_i$ is an active slip-line lengths, $k_i$ a constant which depends on the number of slip systems operating during strengthening, P and $y_i$ are respectively the annihilation probability and distance. One can approximate the local dislocations density established in one phase i of size $d_i$ in steady state ( $d\rho_i = 0$ ) using equation (3) as:

$$\rho_i = \frac{k_i}{2Pd_i y_i} \quad (4)$$

We assume there is a simple relation between the local flow stress and the annihilation distance $y_i = \frac{K_i}{\tau_i}$, without presuming the annihilation process (cross-slip or climb). $K_i$ is a constant which depends on elastic constants, stacking fault energy, temperature and process concerns by the annihilation. Consequently the flow stress in phase i is given by:

$$\tau_i = \frac{2Pd_i K_i}{k_i}\rho_i \quad (5)$$

Shear flow stress $\tau_i$ has been commonly expressed in terms of mean dislocation density in phase i, $\rho_i$ in a Taylor relationship [111, 112] :

$$\tau_i = \alpha_i \mu b \sqrt{\rho_i} \quad (6)$$

The insertion of Eq. (5) into Eq. (6) allows expressing dislocation density as follows:

$$d_i = \left[\frac{k_i}{2\alpha_i \mu b K_i P}\right]\rho_i^{-1/2} \quad (7)$$

This equation is similar to the phenomenological expression found using experimental measurement (Eq. 2) with $d_c=\lambda$ and $d_w=e$. A=B in Eq.2 leads us to conclude that $k_i$, $K_i$ and $\alpha_i$ are less dependent on the phase considered. This relation does not depend on thermodynamical principle but supposes an equilibrium system. Consequently, the similitude principle observed experimentally arises from equilibrium between production and annihilation of dislocations in each phase. The experimental dispersion between the deterministic equation (2) and the experimental results (Figure 13) can be associated with fluctuation of annihilation processes (P) and fluctuation of slip length ($k_i$). In spite of the fact that a large number of pattern sequences (stages II, III, IV, $II_0$, and $III_0$) have been explored in

AISI-316L (Fig. 13b), it is impossible to identify a change of physical mechanism between two sequences using equation (7) (A stays constant), because in the same time, the fluctuations of annihilation process and slip length are probably too large.

***4.3. Scaling regimes and their limitation.***

Scaling behaviour has been observed in many metallurgical systems for properties like the grain sizes [30, 81], dipole heights in cyclic deformed AISI 316L stainless steel [113], fatigue extrusions heights on nickel-base superalloy [114, 115], grain boundaries misorientation and spacing [49-54, 57, 58, 82]. The present study, focused on IDBs, investigates this aspect considering the effect of grain size and grain orientation. Scaling behaviour has been clearly established for the spacing between IDBs ($\lambda$) independently of grain size and grain orientations on nickel when each distribution is normalized by its average value. These results are qualitatively in agreement with previous studies for higher grain sizes and large plastic strains in the same metal [53, 57]. Consequently, within scaling regime, only one parameter $<\lambda>$ governs the evolution of the IDBs for an average spacing range from 300 nm to 1000 nm. A new interesting point is the fact that a normalized distribution is independent of the grain orientation and consequently of the slip activity. This point can be moderated by the fact that IDBs occurrence is observed when slip multiplicity is favoured by grain orientation, or multiaxial stress-strain state in grains which arises to specific loading [97, 98] or to inter-granular plastic strain incompatibilities. This last explanation is well illustrated by the decrease in grain size which promotes slip multiplicity [12]. Consequently, the scaling behaviour observed on $\lambda$ is probably linked to the simultaneity of the activation of more than two systems in the case of IDBs. The physical meaning of the scaling behaviour observed on length scales which characterises dislocation distribution can be explained using statistical mechanics [59, 104, 107-109, 116-118]. The pioneer work of Hähner [104] has been followed by an extensive investigation on the origin of dislocation pattern and the associated scaled distribution. The probability distribution of the total dislocation densities comes from the fluctuation of the dislocation velocity and the effective stress acting on the moving dislocation. The steady-state probability distributions of the scaled dislocation densities derived from stochastic analyses [59, 104] can be used to give a physical explanation of the noise observed on length scales (e and $\lambda$). The distribution of cell size has been easily obtained from the dislocation density distribution using an equation ($\lambda \approx 1/\sqrt{\rho}$) similar to the one previously deduced (Eq. 7) [116, 117]. The distribution of scaled $\lambda$, obtained by stochastic approach, is quite similar to the phenomenological distribution (Eq.1) used to describe our experimental results. The interesting point of this approach is the fact that the noise obtained for the cell size is proportional to the one obtained for the dislocation density. The noise of these distributions depends on the constitutive equations used to account for dislocation multiplication, storage and annihilation processes (by cross-slip or by climb) [104, 107, 116]. A small value of $\sigma^2$ (near 0) corresponds to an homogeneous distribution of dislocations. However, the cross slip facility and easy dislocation recombination under slip multiplicity induce an increase in noise associated with the occurrence of dislocation patterning [116]. These results can be used in the present context. The value of the noise obtained for $\lambda$ (0.08±0.02) is lower than the one which can be deducted from previous results at higher strain in nickel (0.2 for IDBs and 0.33 for GNBs). Thus the physical meaning of the scaling behaviour obtained in the present study is probably different from the one obtained in higher strain. This opinion is confirmed in the following observation. Scaling behaviour is only observed for IDBs thickness on an average thickness range from 80 nm to 120 nm. For the lower value of 80 nm, the noise increases from 0.08 to 0.3. The first value corresponds to the one obtained for IDBs spacing, which confirms a similitude between thickness of walls

and cell size for a given sequence of pattern [62, 119], but the second one is quite similar to the one obtained for GNBs boundaries spacing. Consequently, the physical meaning of the last distribution is probably the same as the one associated with GNBs, or it leads to the same dislocation organisation in the boundary. In other words, the variances 0.08 and 0.3 are associated with a statistical trapping and a deterministic trapping respectively. These observations imply the idea of a progressive transformation of IDBs to GNBs as the plastic strain increases. The reorganisation of dislocations in boundary during strain increase at stage III has been previously suggested as being the reason for the decrease in the fraction of walls observed during this stage. The new physical parameter which can explain this reorganisation is probably the occurrence of climb in IDBs. This opinion is based on the observations of Argon *et al*. [120, 121] on copper which identified annihilation of dislocations associated with climb near walls. Recently, climb has been examined as a possible mechanism to explain dislocation patterns, which seems to confirm the last suggestion [122]. However the progressive transformation of dislocation patterns needs further investigation to clearly demonstrate the role of climb in this process. The noise 0.08 can be correlated to a specific fraction of hard phase (high dislocation density) $f_w$ (e/e+λ) equal to 45%. This last value corresponds to a well-established structure observed at the end of stade II in single crystal well-oriented to multiple slip [67, 68] and in polycrystal [92, 123]. This comment supports the idea that the noise 0.08 is associated with occurrence of multiple slip and generalisation of cross-slip which are the two factors explaining the transition between stage I and stage II. The noise increase (0.08 to 0.3) is easily correlated to the decrease of $f_w$ (45% to 15%), which suggests that a restoration process occurs in walls during stage III in relation to climb of extended dislocations. This progressive transformation modifies the long-range internals stresses occurring in the grain and consequently affects the stress-strain distribution in polycrystalline structure.

[insert Figure 14 about here]

### *4.4. Internal stresses.*

It is now well acknowledged that polycrystalline hardening arises from the evolution of stress-strain fluctuations at microscopic and nanoscopic levels during strengthening. Consequently, the complex stress and strain paths at the "local" level need to be well identified to bridge the gap between the microscopic scale, the mesoscopic scale and the macroscopic scale. TEM observations offer a good opportunity to discuss the interaction between the different levels of heterogeneities. At the mesoscopic scale, two origins of elastic long-range interaction with mobile dislocations have been reported: intra-granular plastic-strain incompatibilities linked to the heterogeneous dislocation distribution and inter-granular strain incompatibilities which result in grain to grain elasto-plastic strain incompatibilities and in the specific behaviour of grain boundary region [28]. In the present part, we'll discuss the role of geometrically necessary dislocations and of long-range internal stresses on the origin of Hall-Petch relationship for the high plastic strains.

**4.4.1 - Geometrically necessary dislocations and Hall-Petch relationship.** Many recent numerical works tried to deal with inter-granular stress fluctuations in terms of statistical point of view, which depend on boundary conditions and constitutive equations used to describe grain behaviour [9, 10, 12, 14, 124-126]. Moreover, one has acknowledged the importance of geometrical dislocation density close to grain boundary on the evolution of inter-granular long-range internal stresses in relation to lattice curvature [9, 11, 127]. These approaches were predictive of Hall-Petch relationship, with an increase in pre-deformation factor k(ε) as a function of plastic strain. This last point is in agreement with different experimental results on the evolution of inter-granular long-range internal stresses for low and

medium plastic strain [28, 62]. However, during the increase in plastic strain for higher values, k(ε) decreases [28, 30], which suggests that the length scale associated with grain boundary is not the predominant factor at larger strain. The decrease of k(ε) and its low value at high plastic strain seem indeed to be correlated to the emergence of patterns in grain. Consequently, the evolution of k(ε) can be linked to a change of length scale. The length scale associated with grain boundary or geometrically necessary dislocations has been the subject of many discussions. Achaya and Baudoin [11] proposed a phenomenological relation between mean free paths determined by geometric obstacles and slip plane lattice incompatibility characterized by a non-dimensional parameter $k_0$. No information on the location on the geometric obstacles and to the physical meaning of $k_0$ was provided by the authors. In a similar trend, Forest and his co-workers [9, 10] used Cosserat single crystal plasticity in multi-crystalline aggregates to describe the influence of grain size on hardening behaviour of polycristals. The Hall-Petch type relation is well explained in terms of lattice curvature. Moreover, plastic curvature does not develop in the core of the grain but at the grain boundaries [9]. This means that the contribution of geometrically necessary dislocation is predominant only near grain boundaries. This region is characterized by a length $l_p$ introduced in the phenomenological constitutive equation of the lattice curvature. In a way similar to the approach proposed by Achaya and Baudoin [11], $l_p$ has no physical basis. An alternative for these studies was proposed using discrete dislocation dynamic [13, 18, 19]. The Hall-Petch's relation is well predicted with these approaches with an accumulation of dislocations near grain boundaries which are sometimes understood as geometrically necessary dislocations [19]. In the state of these studies, the nature and mechanism which occur in grain boundary are not or less taken into account and no length scale has been evaluated. The fact that Hall-Petch relationship results in pile-up process and/or in geometrically necessary dislocations remains an open question. However, experimental investigations on f.c.c. alloys have clearly established the fact that pile-ups disappear at the hardening transition between stage I and stage II [28, 62] and consequently cannot explain the Hall-Petch relation for higher strains. Following the models of Hirth [6] and Meyers [7], the grain can be assumed to be a composite microstructure composed of grain core (GC), surrounded by hard grain-boundary (GB) with thickness t. This approach, which shows a good Hall-Petch relationship, has been recently explored to study the evolution of inter-granular back stress at early stage of plastic strain [28]. With an access to the dislocation densities in grain and in the vicinity of grain by TEM [89], the composite model provides a good approach of the reduction of inter-granular long-range internal stresses for large grain sizes which result in a reduction of the difference observed between dislocation densities in GB and GC [28]. This homogenization of total dislocation density has been observed to occur near 6% of plastic strain in austenitic stainless steel but at the same time inter-granular long-range internal stresses do not disappear [28, 89]. These results have been derived from a model assuming an empirical law for length scale t: $t = k \times d^{-1/2}$ [7]. This law has no physical basis but can be identified using experimental results [7, 28]. Moreover, we have supposed in this approach that grain size affects only inter-granular internal stresses. This assumption is open to criticism. To sum up all these studies, it can be said that the Hall-Petch relationship which is related to a gradient of dislocation densities (geometric or not) cannot be sufficient to explain this relation on large strains for two reasons: no difference is observed between dislocation density measured in grain vicinity and grain core at large strain, and inter-granular long-range internal stresses partially persist in high strain. We explore the assumption that the possible dependence of intra-granular long-range internal stresses on inter-granular long-range internal stresses can be explained by the persistence of Hall-Petch relation in large strain.

**4.4.2 - Inter-granular and intra-granular long-range internal stresses.** In the present work the mean value of intra-granular long-range internal stress $<X_{intra}>$ which arises in grain in relation to dislocation patterning has been evaluated using the composite model initially proposed by Mughrabi [128]. Details of this calculation are given in former publications [62, 128]. The spatial arrangement of dislocations in each grain is determined in terms of dislocation densities in soft phases $\rho_s$ (channels) and hard phases $\rho_w$ (walls) and the fraction of hard phase $f_w$ is calculated.$<X_{intra}>$, is a mean value of long-range internal stresses experienced by mobile dislocations in inter-walls spacing. The crude approach which does not take into account the geometrical aspect of dislocation pattern allows an evaluation of $<X_{intra}>$ as follows:

$$< X_{\text{int } ra} >= M < f_w > \alpha\mu b(\sqrt{< \rho_w >} - \sqrt{< \rho_s >}) \quad (8)$$

where $\alpha$ is a constant depending on the elastic interaction of dislocations ($\alpha$=0.4 [2]) and M is a Taylor factor. The evaluation of $<X_{intra}>$ has been performed as a function of grain orientation for two grain sizes in nickel. Figures 14a and 14b point out the fact that three domains can be defined on stereographic triangle where $<X_{intra}>$ fluctuations in each domain are lower than 10%. These domains correspond to the ones defined in terms of pattern type (I, II or III) and/or microstructural parameters (e, $\lambda$). If we consider larger grain size (168 µm, Figure 14b) $<X_{intra}>$ depends on grain orientation with the following sequence: type I<type II<type III. Consequently, the fact that single slip orientations (type I) less favor IDBs formation than multiple slip orientations (types II and III) induces a lower value of intra-granular long-range internal stress in type I orientation than the ones obtained in the other orientations. The idea that the intra-granular stress-strain field is only determined by grain orientation can be refused with the results obtained for low grain size (18 µm, figure 14a). If $<X_{intra}>$ depends on grain orientation, it also depends on grain size for specific orientations. Type I and type II orientations seem less dependent on grain size. However, $<X_{intra}>$ is decreased when the grain size decreases for type III grain orientations. This result is in opposition with the assumption that the grain size affects only inter-granular long-range internal stress [28].

**4.4.3 - Internal stresses and Hall-Petch relationship.** The last comment can be confirmed using the comparison between the mean values of $X_{intra}$ obtained for one grain size $\overline{X}_{\text{int } ra}$ (mean value obtained on the population of grains studied for one grain size) with the one deduced from Hall-Petch analysis which assumes that only inter-granular long-range internal stress is affected by grain size [28]. Irrespective of the stacking fault energy, both stresses are quite similar for high grain size, which seems to valid the previous assumption (Table 1). However, for lower grain size considered in nickel (18 µm), a large difference is observed between the two evaluations of $\overline{X}_{\text{int } ra}$: the Hall-Petch approach predicts a higher value than the one using TEM measurement. Consequently, some parts of inter-granular long-range internal stress can probably be independent from the grain size. This last result is in agreement with the existence of two origins of inter-granular plastic strain incompatibilities: the strain gradient which arises near grain boundary and the elasto-plastic interaction between grains associated with their different crystallographic orientations. If the former depends on the grain size, the latter has no reason to be affected by it. Moreover, intra-granular back stress $\overline{X}_{\text{int } ra}$ decreases as a function of the decrease in grain size, which means that either the grain size or the length scale associated with it affect the dislocation patterning and consequently $\overline{X}_{\text{int } ra}$. This effect can be understood as a plastic strain history. The grain size and more precisely the inter-granular part of long-range internal stresses which depend on the grain size modify the local strain path in grain during tensile loading. The dislocation pattern

developed on grain depends on this local strain path and consequently on the grain size. Thus, the dependence of intra-granular long-range internal stresses on the grain size arises naturally in the strain path history. This effect does not seem to be valid in the case of a high grain size, which gives support to the theory of the existence of a threshold grain size under which an interaction between inter-granular and intra-granular takes place. This threshold is probably equal to $d_c$ which is the qualitative expression of the transition between equiaxed cells independent of the grain orientation and pattern which depend on this orientation (Figure 4). Moreover, $d_c$ can also be interpreted as a length scale associated with grain boundary vicinity.

[insert table 1 about here]

## 5. Conclusion.

The influence of strain incompatibility on the activation of multiple slips is well known, but its incidence on patterning has been less studied in the polycrystals. We have shown here that the nature of the dislocations cells depended on the grain size and on the crystallographic orientation with respect to the occurrence of multiple slip. The dimensional parameters (e, λ) are classified in three fields of crystallographic orientation but are also a function of the grain size. In other words, the interactions between inter-granular and intra-granular incompatibilities increase as the size of the grain decreases. Thus the assumption that intra-granular long-range internal stresses do not depend on the grain size for large plastic strains [28] becomes erroneous for low grain sizes. The Hall & Petch phenomenological law at a high strain is a consequence of plastic strain history effect and of the strain gradient in grain which affects intra-granular long-range internal stresses. Moreover, at the strain level considered in this work (~30%), two sequences of patterning have been identified in terms of specific noise associated with length scales λ and e.

## Bibliographies

[1] R.W. Armstrong, I. Cood, R.M. Douthwaite and N.J. Petch, Phil. Mag. A, **7**, 45 (1962).
[2] J.C.M. Li, Trans. Met. Sco., **227**, 239 (1963).
[3] M.F. Ashby, Phil. Mag. *A*, **21**, 299 (1970).
[4] J.C.M. Li and Y.T. Chou, Met. Trans., **1**, 1145 (1970).
[5] H., Conrad, *in Ultrafine-Grain Metals,* edited by J.J. Burke and V. Weiss (Syracuse University Press, 1970) p. 213.
[6] J.P. Hirth, Metall. Trans., **3**, 3047 (1972).
[7] M.A. Meyers and E. Ashworth, Phil. Mag. A, **46,** 737 (1982).
[8] R.W. Armstrong, *Field, Flow and Fracture of polycristals*, edited by T.N. Backer (Applied Science, 1983),.
[9] S., Forest, Mat. Res. Soc. Proc., **653**, Z8.2.1 (2001)
[10] S. Forest, Int. J. of Sol. and Struc., **37**, 7105 (2000).
[11] A. Acharya and A.J. Beaudouin, J. of the Mech. and Phys. of Sol., **48**, 2213 (2000).
[12] F. Barbe, S. Forest and G. Cailletaud, Int. J. of Plast., **17**, 537 (2001).
[13] J. Aldazabal and J. Gil Sevillano, Z. Metallkd, **93**, 981 (2002).
[14] G. Cailletaud, S. Forest, D. Jeulin, F. Feyel, I. Galliet, V. Mounoury, S. Quilici, Comp. Mat. Sc., **27**, 351 (2003).
[15] H. Conrad, Mat. Sci. and Eng. A, **341**, 216 (2003).
[16] H. Conrad, Met. Trans. A, **35A**, 2681 (2004).
[17] H. Conrad and K. Jung, Mat. Sci. And Eng. A, **391**, 272 (2005).
[18] S.B. Biner and J.R. Morris, Phil. Mag., **83**, 3677 (2003).
[19] D.S. Balint, V.S. Deshpande, A. Needleman, E. Van der Giessen, Mater. Sci. and Eng. A, **400-401**, 186 (2005).
[20] V. Bata and E.V. Pereloma, Acta Mater., **52**, 657 (2004).
[21] S. Lefebvre, B. Devincre and T., Hoc, Mat. Sci. and Eng. A, **400-401,**150.
[22] G. Saada, Phil. Mag., **85**, 3003 (2005a).

[23] G. Saada, Mat. Sci. and Eng. A, **400-401**, 146 (2005b).
[24] H. Fujita and T. Tabata, Acta Met., **21**, 355 (1973)**.**
[25] T. Tabata, K. Takagi and H. Fujita, Trans. JIM, **26**, 569 (1975)**.**
[26] N. Hansen, Acta Met*.,* **25**, 863 (1977)**.**
[27] N. Behnood and J.T. Evans, Mat. Sci. and Eng. A, **55**, 263 (1982)**.**
[28] X. Feaugas and H. Haddou, Met. Trans. A, **34A**, 2329 (2003a).
[29] H. Mecking, *in Defomation in polycristals*, edited by N. Hansen *et al.* (Riso National Laboratory, Denmark, 1981) 73.
[30] H. Haddou, Doctoral thesis, UTC, Compiègne, France (2003).
[31] J.G. Rao and S.K. Varma, Met. Trans. A, **24A**, 2559 (1993).
[32] D. Sil and S.K. Varma, Met. Trans. A, **24A**, 1153 (1993).
[33] Q. Liu and N. Hansen, Phys. Stat. sol. (a), **149**, 187 (1995).
[34] N. Hansen and X. Huang, Acta. Mater., **46**, 1827 (1998).
[35] N. Hansen, X. Huang and D.A. Hughes, Mater. Sci. and Eng. A, **A317**, 3 (2001).
[36] X. Huang and N. Hansen, Scripta Mater., **37**, 1 (1997).
[37] X. Huang, Scripta Mater., **38**, 1697 (1998).
[38] X. Huang, A. Borrego and W. Pantleon, Mater. Sci. and Eng. A, **A319-321**, 237 (2001).
[39] X. Huang and N. Hansen, Mater. Sci. and Eng. A, **A387-389**, 186 (2004).
[40] X. Feaugas, HDR thesis*,* UTC, France (1999a).
[41] G. Winter, X. Huang and N. Hansen, *Acta Mater.,* **48**, 2187 (2000).
[42] G. Winter, Mat. Sci. and Eng. A, **309-310**, 486 (2001).
[43] C. Gaudin, Doctoral thesis, UTC, France (2002)**.**
[44] C. Buque, J. Bretschneider, A. Schwab, C. Holste, Mat. Sci. and Eng. A, **A300**, 254 (2001)**.**
[45] C. Gaudin and X. Feaugas, Mat. Sci. and Eng. A, **A209-310**, 382 (2001).
[46] A. Schwab and C. Holste, Acta Mater., **50**, 289 (2002).
[47] C. Holste, Phil.Mag., **84**, 299 (2004).
[48] X. Feaugas and C. Gaudin, Acta Mater., **52**, 3097 (2004b).
[49] D.A. Hughes, Q. Liu, D.C. Chrzan, N. Hansen, Acta Mater., **45**, 105 (1997a).
[50] D.A. Hughes and N. Hansen, Acta Mater., **45**, 3871 (1997b).
[51] D.A. Hughes, D.C. Chrzan, Q. Liu, N. Hansen, Phys. Rev. Lett., **81**, 4664 (1998).
[52] D.A. Hughes and N. Hansen, Phys. Rev. Lett*.,* **87,** 135 (2001).
[53] D.A. Hughes and N. Hansen, Acta Mater., **48**, 2985 (2000).
[54] D.A. Hughes, Scripta Mater., **47**, 697 (2002) .
[55] D.A. Hughes and N. Hansen, Phil. Mag., **83**, 3871 (2003a).
[56] D.A. Hughes, N. Hansen, D.J. Bammann, Scripta Met., **48**, 147 (2003b).
[57] A. Godfrey and D.A. Hughes, Acta Mater., **48**, 1897 (2000).
[58] A. Godfrey and D.A. Hughes, Scripta Mater., **51**, 831 (2004).
[59] M. Zaiser and A. Seeger, *in Dislocation in Solids*, **11**, edited by F.R.N. Nabarro and M.S. Duesbery (Elsevier publisher, 2002) 1.
[60] H. Haddou, C. Gaudin, X. Feaugas, J. Phys. IV, **11**, Pr4-283 (2001).
[61] H. Haddou, M. Risbet, G. Marichal and X. Feaugas, Mater. Sci. and Eng. A, **A379**, 102 (2004).
[62] X. Feaugas, Acta Mater., **47**, 3617 (1999b).
[63] R. Neuhaus, P., Buchhagen, C., Schwink, Scripta Met., **23**, 779 (1989).
[64] E. Underwood, *Quantitative stereology* (Addison-Wesley Publishing Compagny, 1970).
[65] J.W. Steeds, Proc. Roy. Soc., **A292**, 343 (1965).
[66] M.R. Staker and D.L. Holt, Acta Met., **20**, 59 (1979).
[67] E. Göttler, Phil. Mag A., **28**, 1057 (1973).
[68] P. Ambrosi, E. Göttler and C. Schwink, Scripta Met., **8**, 1093 (1974).
[69] H. Mughrabi, *in Constituve equations in plasticity*, edited by A.S. Argon (MIT press Cambridge, 1975) p. 199.
[70] Y. Kawasaki, J. of Appl. Phys., **18**, 1429 (1979).
[71] Y. Kawasaki, Scripta Met., **14**, 183 (1980).
[72] Y. Kawasaki, *ICSMA1*0, edited by S. Oikawa et al. (The Japan Institute of Metals, 1994) p. 187.
[73] E.S. Kayali and A. Plumtree, A., Metall. Trans. A, **13A**, 1033 (1989).
[74] T. Narutani and J. Takamura, Acta. Met., **39**, 2037 (1991).
[75] R. Neuhaus and C. Schwink, Phil. Mag. A, **65**, 1463 (1992).
[76] X. Feaugas, Phys. stat. sol. A*,* submitted (2006).
[77] H. Fujita and S. Kimura*,* J. of the Phys. So. of Japan, **52**, 157 (1983).
[78] G. Winter, D. Juul Jensen and N. Hansen, Acta Mater*.,* **45**, 5059 (1997).
[79] Q. Liu, D. Juul Jensen and N. Hansen, Acta Mater., **46**, 5819 (1998).

[80] R. McCabe, A. Misra and T.E. Mitchell, Acta Mater., **52**, 705 (2004).
[81] F.J. Humphreys and M. Hartherly, *Recrystallization and related annealing phenomena* (Oxfrod, Pergamon Press, 1995).
[82] W. Pantleon and N. Hansen, Acta Mater., **49**, 1479 (2001).
[83] H. Mughrabi, Mat. Sci. and Eng. A, **85**, 15 (1987).
[84] A.S. Argon, Scripta. Met., **47**, 683 (2002).
[85] R. Madec, B. Devincre and L.P. Kubin, Scripta Met. **47**, 689 (2002).
[86] H. Fujita, N. Sumida, S. Kimura and T. Takemoto, J. of the Phys. So. of Japan, **51**, 577 (1982).
[87] P.J. Jackson, *in Dislocations and Properties of real Materials* (The institute of Metals, London, 1985) p. 44.
[88] G. Winter, Acta Mater., **51**, 417 (2003).
[89] M. Janecek and K. Tangri, Mat. Sci. And Eng. A., **138**, 237 (1991).
[90] M. Janecek and K. Tangri, J. Mater. Sci., **30**, 3820 (1995).
[91] G. Cailletaud, Inter. J. of Plasticity, **8**, 55 (1992).
[92] X. Feaugas, Rec. Res. Dev. in Mater. Sci., **4**, 35 (2003).
[93] K. Hashimoto and H. Margolin, Acta Metall., **31**, 773 (1983).
[94] K. Hashimoto and H. Margolin, Acta Metall., **31**, 787 (1983).
[95] H. Margolin, Z. Wang and T.K. Chen, Metall. Trans. A, **17A**, 107 (1986).
[96] C. Zhao and H. Margolin, Met.Trans. A, **19,**1575 (1988).
[97] M. Clavel and X. Feaugas, Micromechanisms of plasticity under multiaxial cyclic loading, *in Multiaxial Fatigue and Design, ESIS 21*, edited by A. Pineau, G. Cailletaud and T.C. Lindley, (Mechanical Engineering Publications, London, 1996) p. 21.
[98] L. Bochet, P. Delobelle, P. Robinet and X. Feaugas, Int. J. of Plasticity, **17**, 1491 (2001).
[99] F.R.N. Nabarro, Mat. Sci. Eng. A, **80**, 759 (2001).
[100] D. Kuhlmann-Wilsdorf and H. Nine, H., J. Appl. Phys., **38**, 1683 (1967).
[101] D. Holt, J. Appl. Phys., **4**1, 3197 (1970).
[102] D. Walgraef and E.C. Aifantis, J. Appl. Phys., **58**, 688 (1985).
[103] N. Hansen and D. Kuhlmann-Wilsdorf, Mater. Sci. and Eng. A, **81**, 141 (1986).
[104] P. Hähner, Acta Mater., **44**, 2345 (1996).
[105] I. Groma and P. Balogh, Acta Mater., **47**, 3647 (1999).
[106] F.R.N. Nabarro, Phil Mag. *A,* **317**, 12 (2000).
[107] P. Hähner, Scripta Mater., **47**, 415 (2002).
[108] R. Thomson, M. Koslowski and R. LeSar, Phys. Letters A, **332**, 207 (2004).
[109] A.H.W. Ngan, Scripta Met., **52**, 1005 (2005).
[110] U. Essmann and H. Mughrabi, Phil. Mag. A, **40**, 731 (1979).
[111] P.B. Hirsch, *in Internal stresses and Fatigue in Metals*, edited by G.M. Rassweiller and W.L. Grube (Elsevier, 1959) p. 139.
[112] G. Saada, Acta Metall., **8**, 841 (1960).
[113] S. Catalao, X. Feaugas, P. Pilvin and M.T. Cabrillat, Mater. Sci. and Eng. A, **400-401**, 349 (2005).
[114] M. Risbet and X. Feaugas, *in EMMC9*, France (2006a).
[115] M. Risbet, X. Feaugas, C. Guillemer-Neel and M. Clavel, *in 9th Int. Fatigue Congress*, Atlanta, USA (2006b).
[116] P. Hähner, Mat. Sci. and Eng. A., **271**, 443 (1999).
[117] M. Zaiser, Mat. Sci. and Eng. A, **249**, 145 (1998).
[118] M. Zaiser, Mat. Sci. and Eng. A, **309**,304 (2001).
[119] D. Knoesen and S. Kritzinger, Acta Metall., **30**, 12119 (1982).
[120] A.S. Argon and W.C. Moffat, Acta Metall, **29**, 293 (1981).
[121] F. Prinz, A.S. Argon and W.C. Moffatt, Acta Metall., **30**, 830 (1982).
[122] B. Bako, I. Groma, G. Györgyi and G. Zimanyi, 2006, Comp. Mat. Sci., to be published (2006).
[123] B.P. Kashyap, K. McTaggart and K. Tangri, Phil. Mag. A, **57**, 97 (1988).
[124] S. Quilici and G. Cailletaud, Comp. Mat. Sci., **16**, 383 (1999).
[125] C. Wei, S. Lin, R.G. Qian and J.M. Hsiao, Acta Metall., **39**, 2051 (1991).
[126] F. Havlicek, M. Tokuda, S. Hino and J. Kratochvil, Inter. J. of Plast., **8**, 477 (1992).
[127] A. J. Beaudoin, A. Acharya, S.R. Chen, D.A. Korzekwa and M.G. Stout, Acta Mater., **48**, 340 (2000).
[128] H. Mughrabi, Acta Metal. Mater., **31**, 1367 (1983).
[129] N. Hansen and B. Ralph, Acta Met., **30**, 411 (1982).
[130] J.J. Gracio, V. Fernandes and J.H. Schmitt, Mater. Sci. Eng. A, **118**, 97 (1989).
[131] A.W. Thomson, M. Baskes and F. Flanagan, Acta Met., **21,** 1017 (1973).
[132] H. Mughrabi, Phil. Mag., **86**, 1 (2006).

.

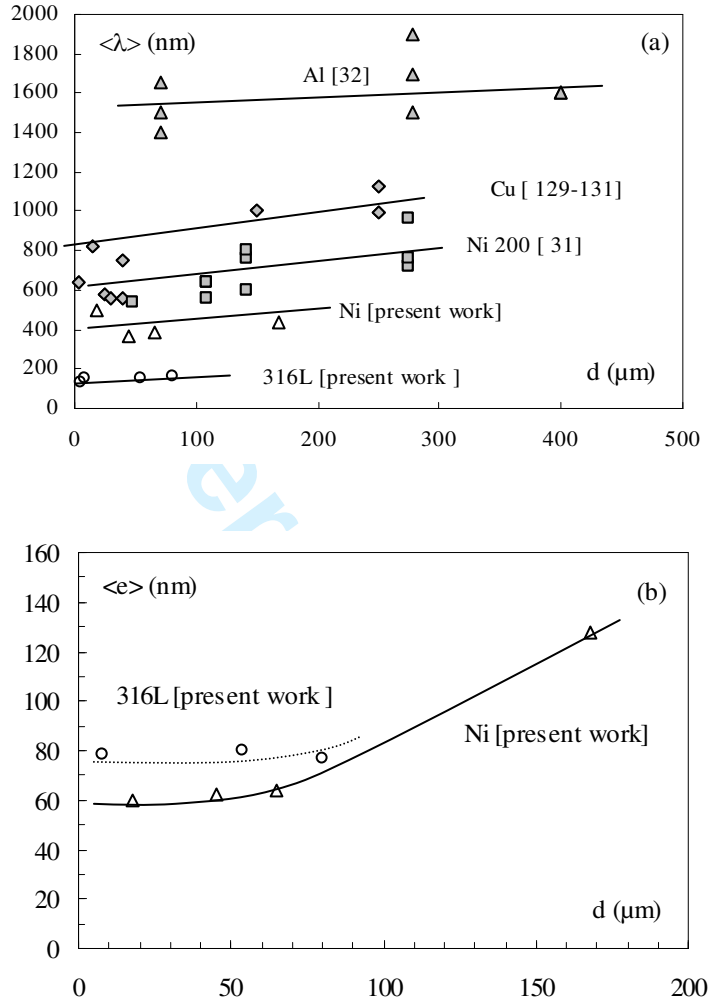


Figure 1 : Average values of inter-walls spacing <λ> (a) and boundary thickness <e> (b) as a function of grain size for IDBs boundaries at a plastic strain equal to 0.3±0.04.

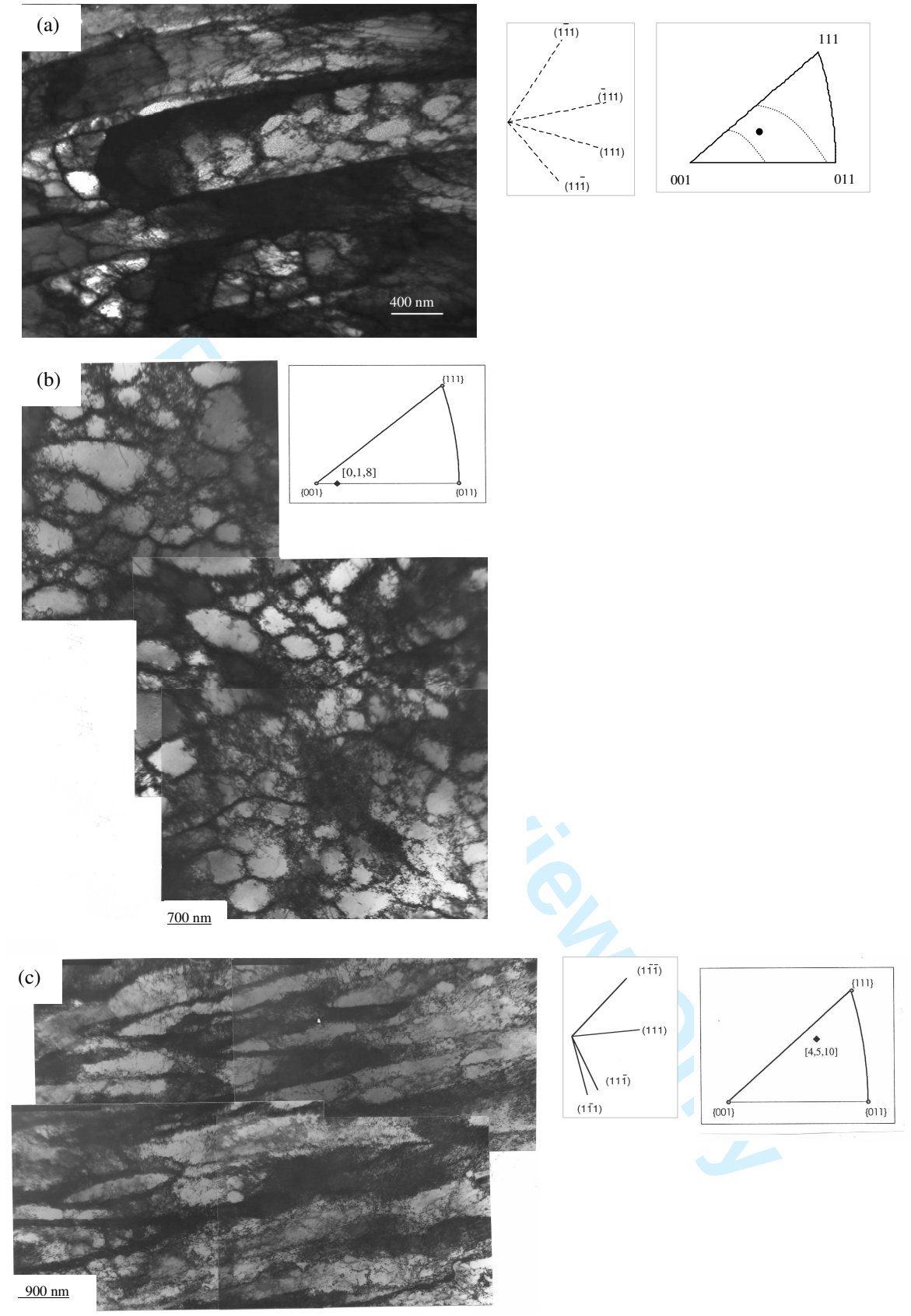


Figure 2: Dislocation patterns observed in stage III for f.c.c. metals ($\varepsilon_p$=0.3). (a) Type I microstructure is subdivided by extended straight GNBs on $(\bar{1}\,11)$. Between these boundaries, quite equiaxed cells are formed to IDBs. (b) Type II: equiaxed cells without specific crystallographic orientations. (c)Type III: long-cells with non-crystallographic boundaries.

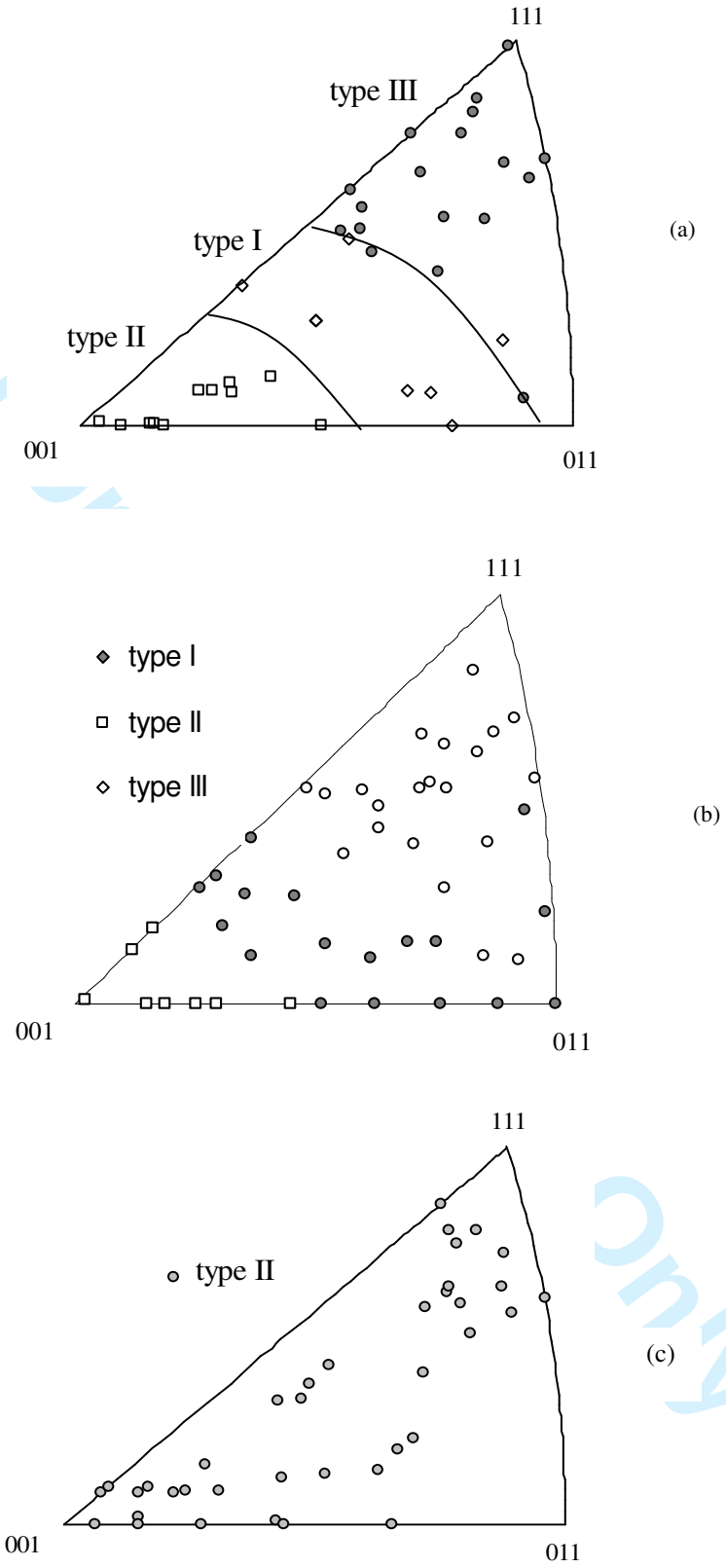


Figure 3 : The different types of cell structures observed are presented on inverse poles figures. The position of one grain is defined by the orientation of tensile axis on inverse pole figure. (a) Inverse pole figures for Ni-D (d=168µm), (b) Inverse pole figure for austenitic stainless steel (d=53µm), (c) Inverse pole figure for Ni-A (d=18µm).

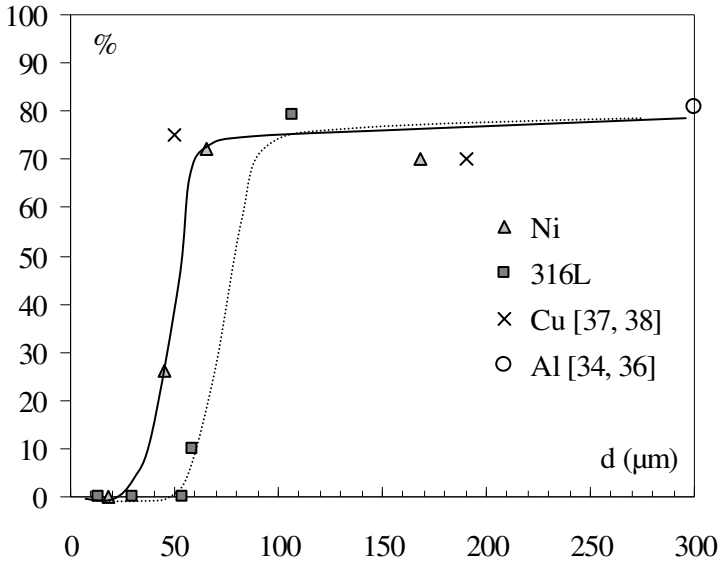


Figure 4: Fraction of long-cells (type I and type III) as a function of grain size (stages II and III).

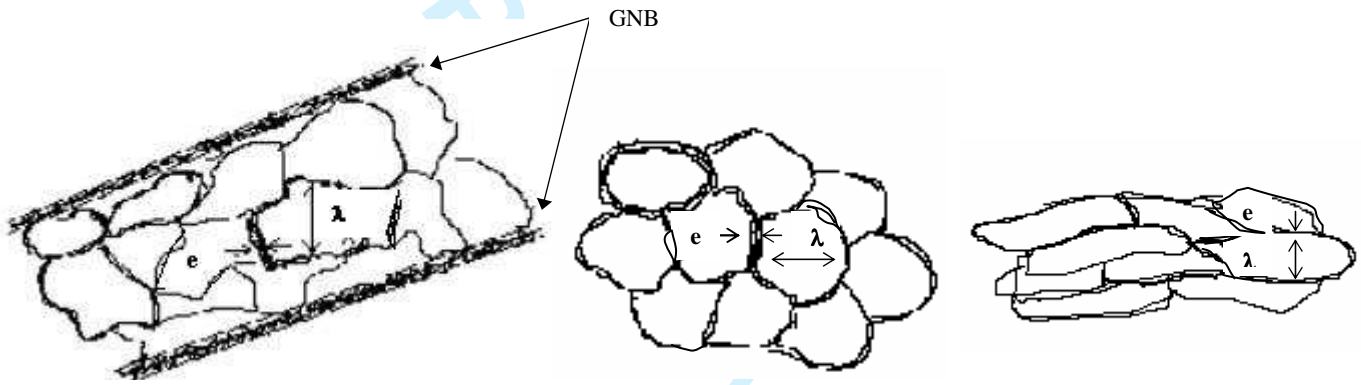


Type I (a) Type II (b) Type III (c)

Figure 5: Different structural characteristic used to investigate IDBs in each dislocation patterns: (e) the boundary thickness and (λ) the inter-boundary spacing.

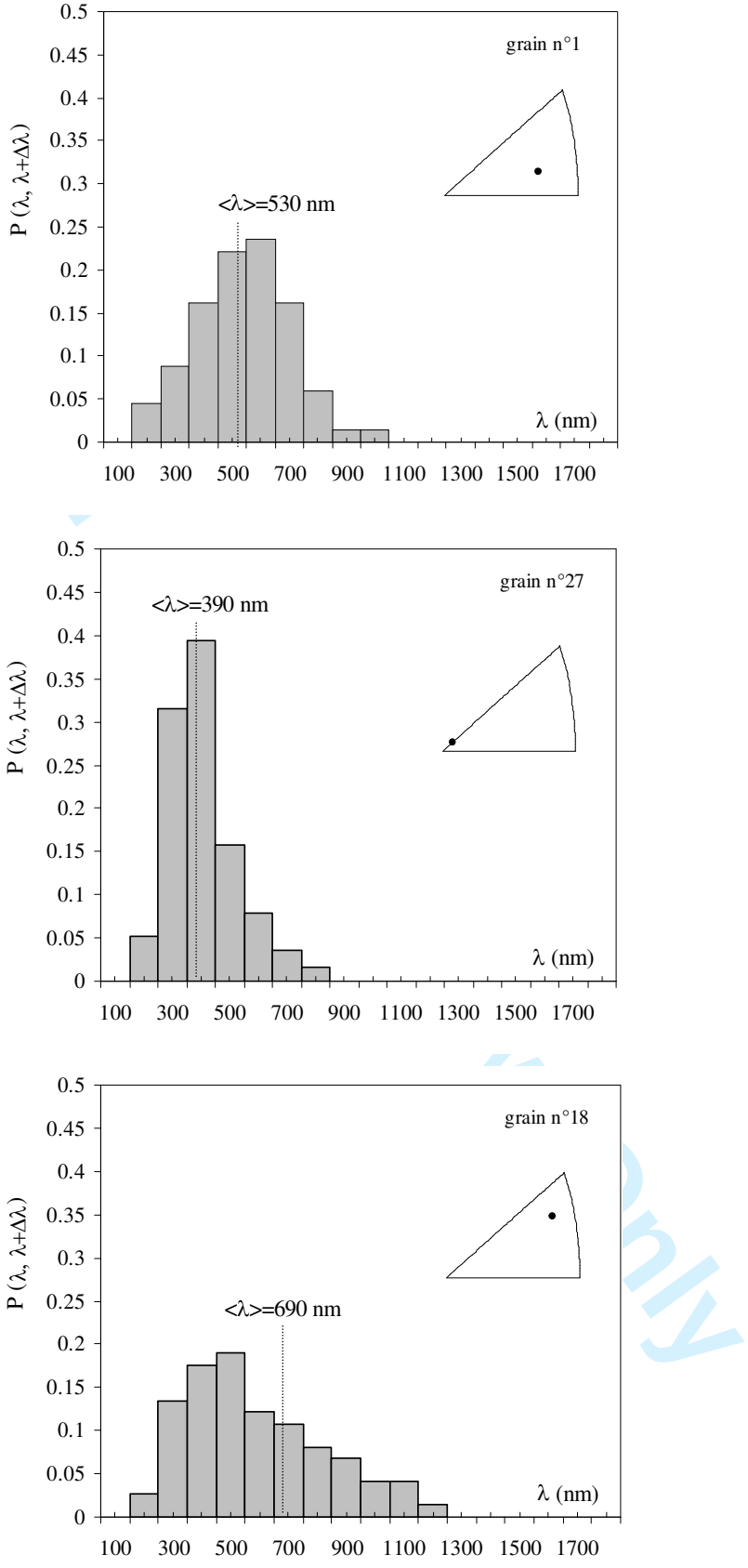


Figure 6: The probability densities of the IDB spacing (λ) for different grain orientations in Ni-A (d=18μm). Only type II microstructure is observed.

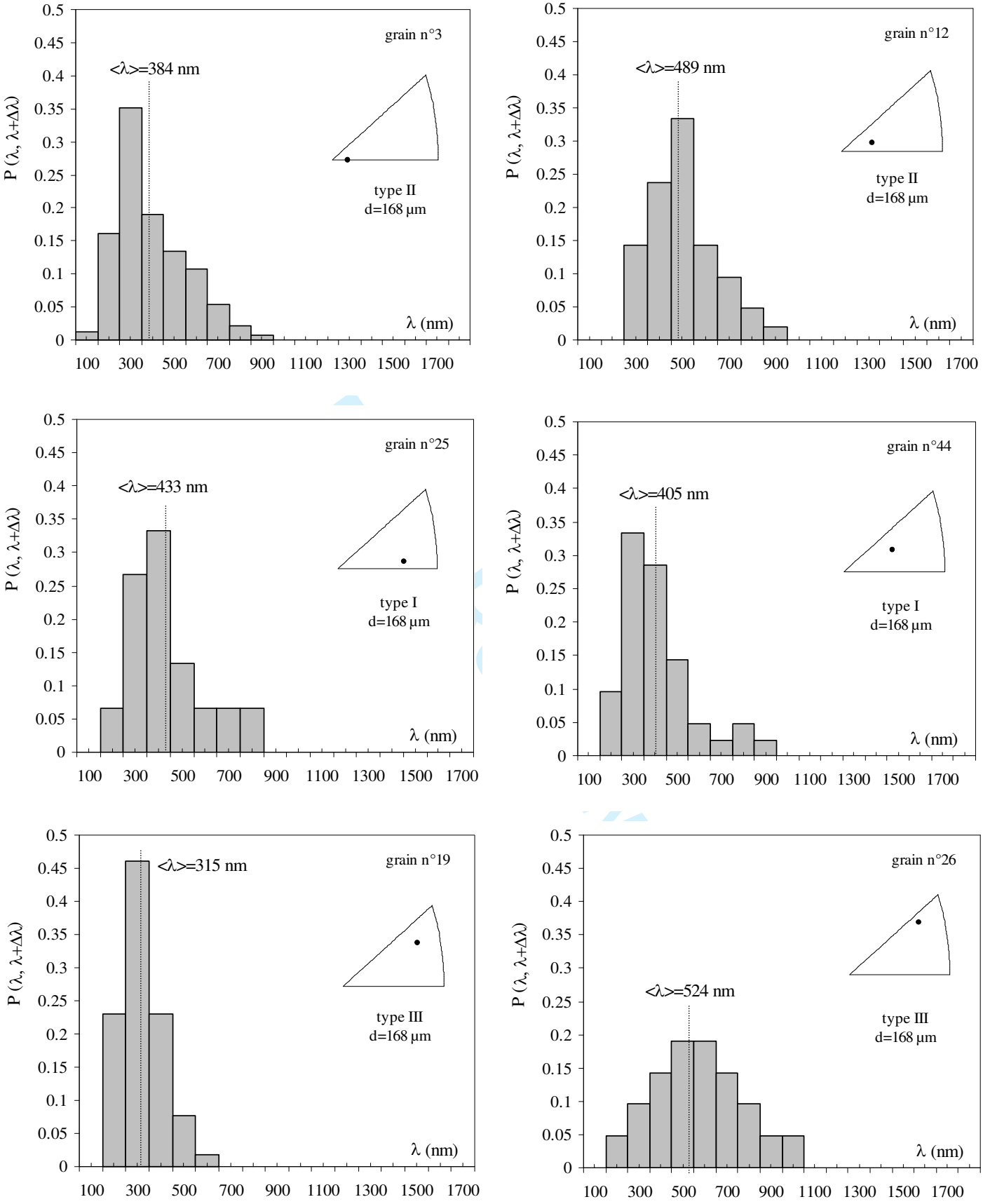


Figure 7: The probability densities of the IDB spacings (λ) for different grain orientations in Ni-D (d=168µm).

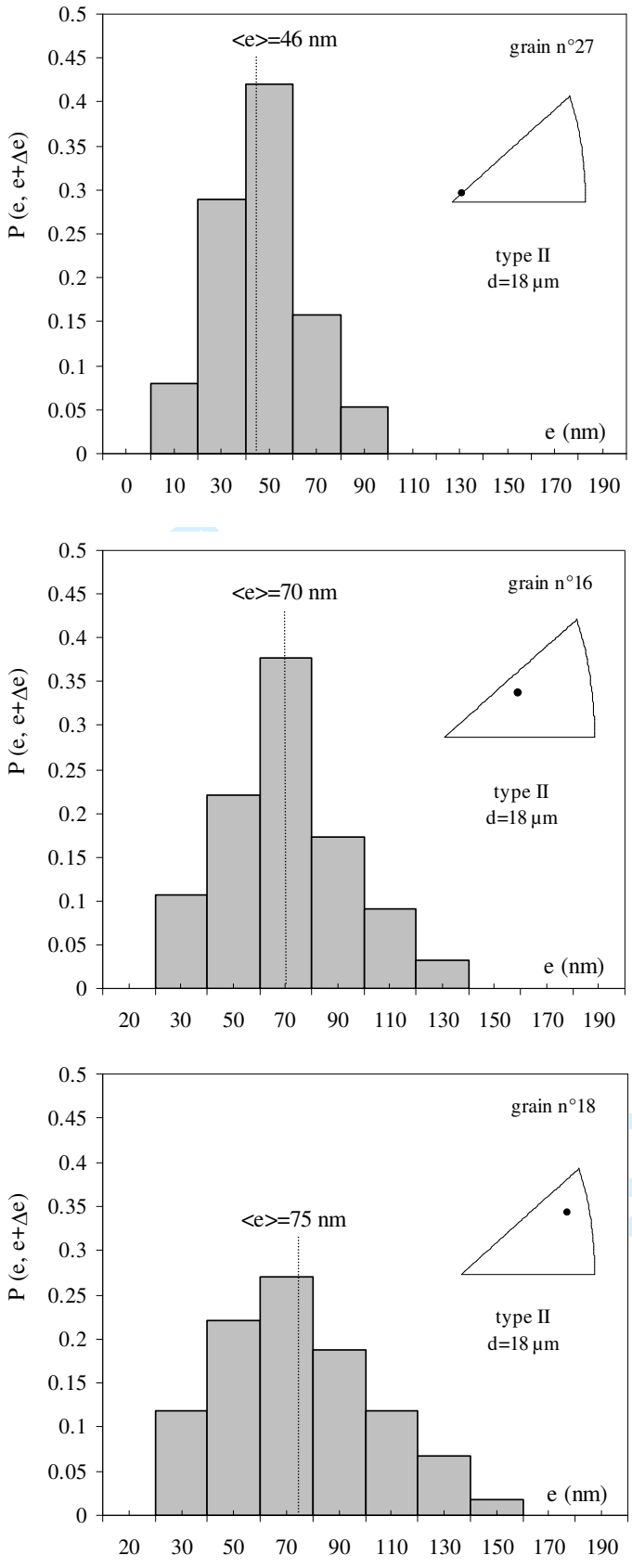


Figure 8: The probability densities of the IDB thickness (e) for different grain orientations (Type II microstructure, Ni-A d=18µm).

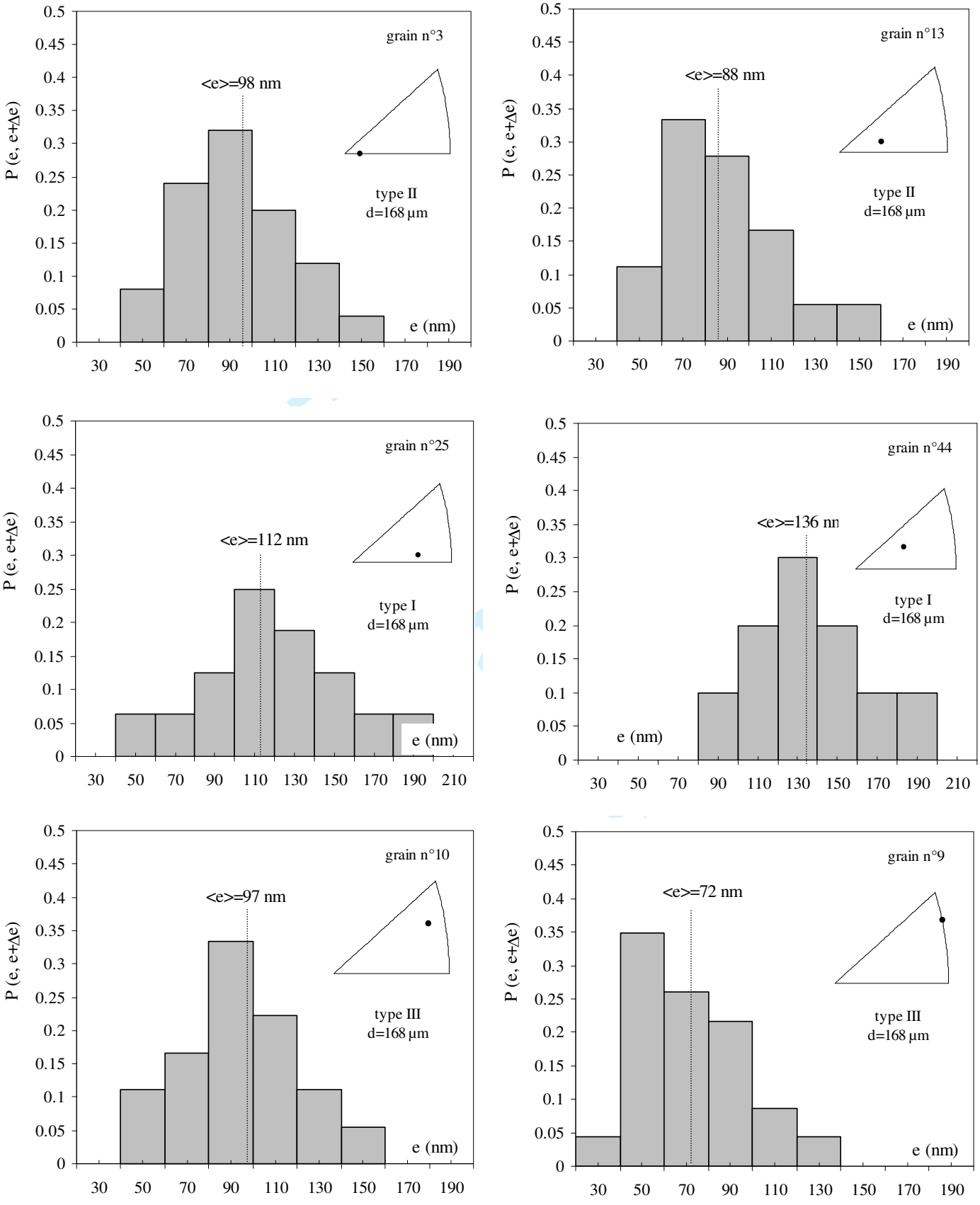


Figure 9: The probability densities of the IDB thickness (e) for different grain orientations in Ni-D (d=168µm).

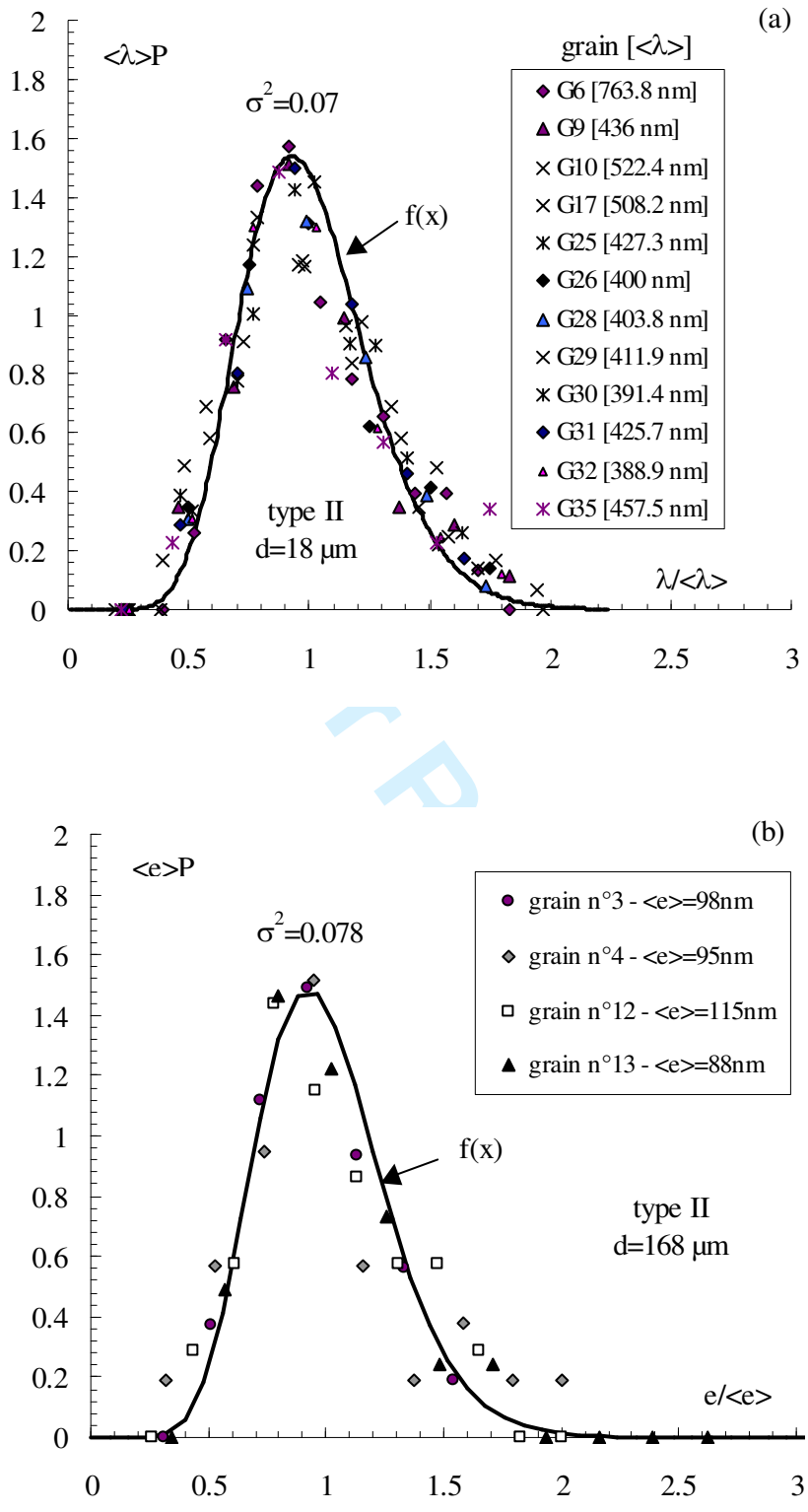


Figure 10: Example of the probability density functions of IDB spacing (a) and IDB thickness (b) normalized respectively by the average spacing and thickness obtained for different grain size and grain orientation. Both distributions are scaled to the similar function f(x) with a noise $\sigma^2$.

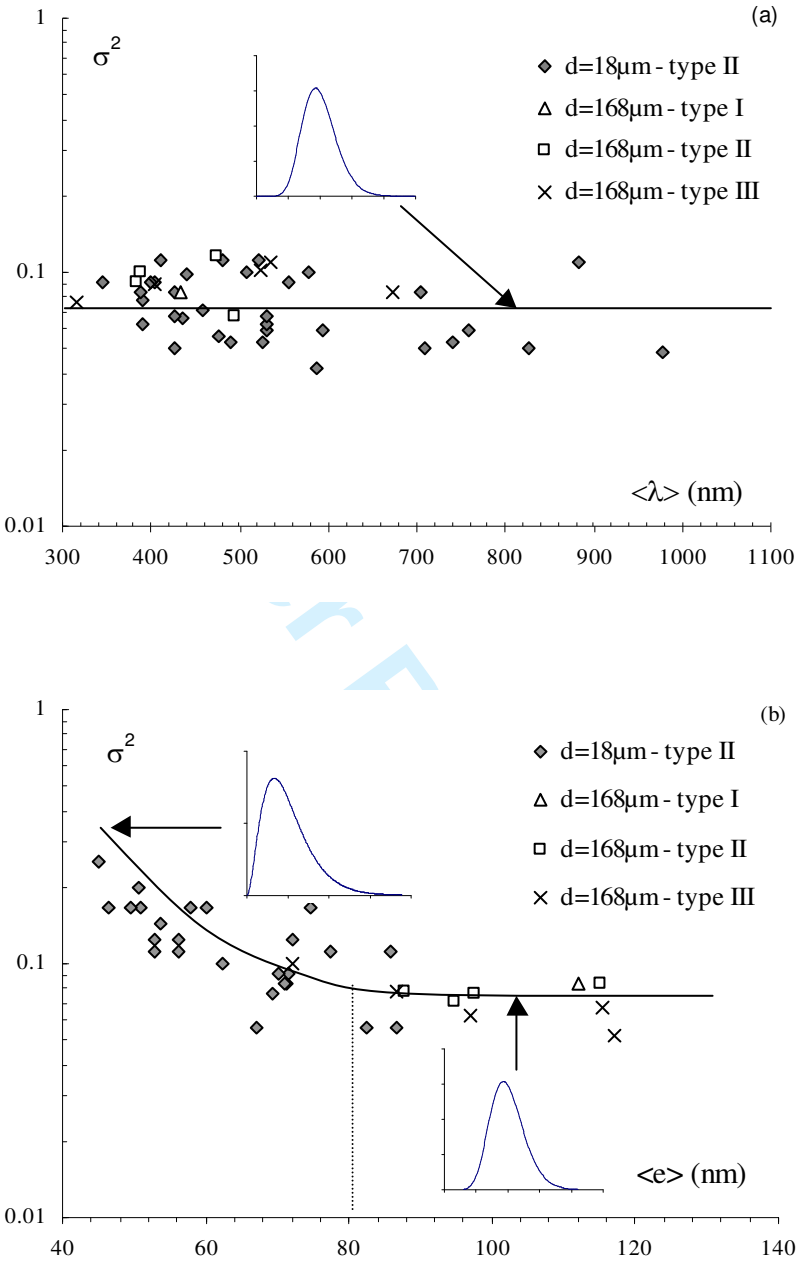


Figure 11: Noise $\sigma^2$ of spacing (a) and thickness (b) distributions as a function of respectively average IDB spacing and IDB thickness. Each point corresponds to one grain.

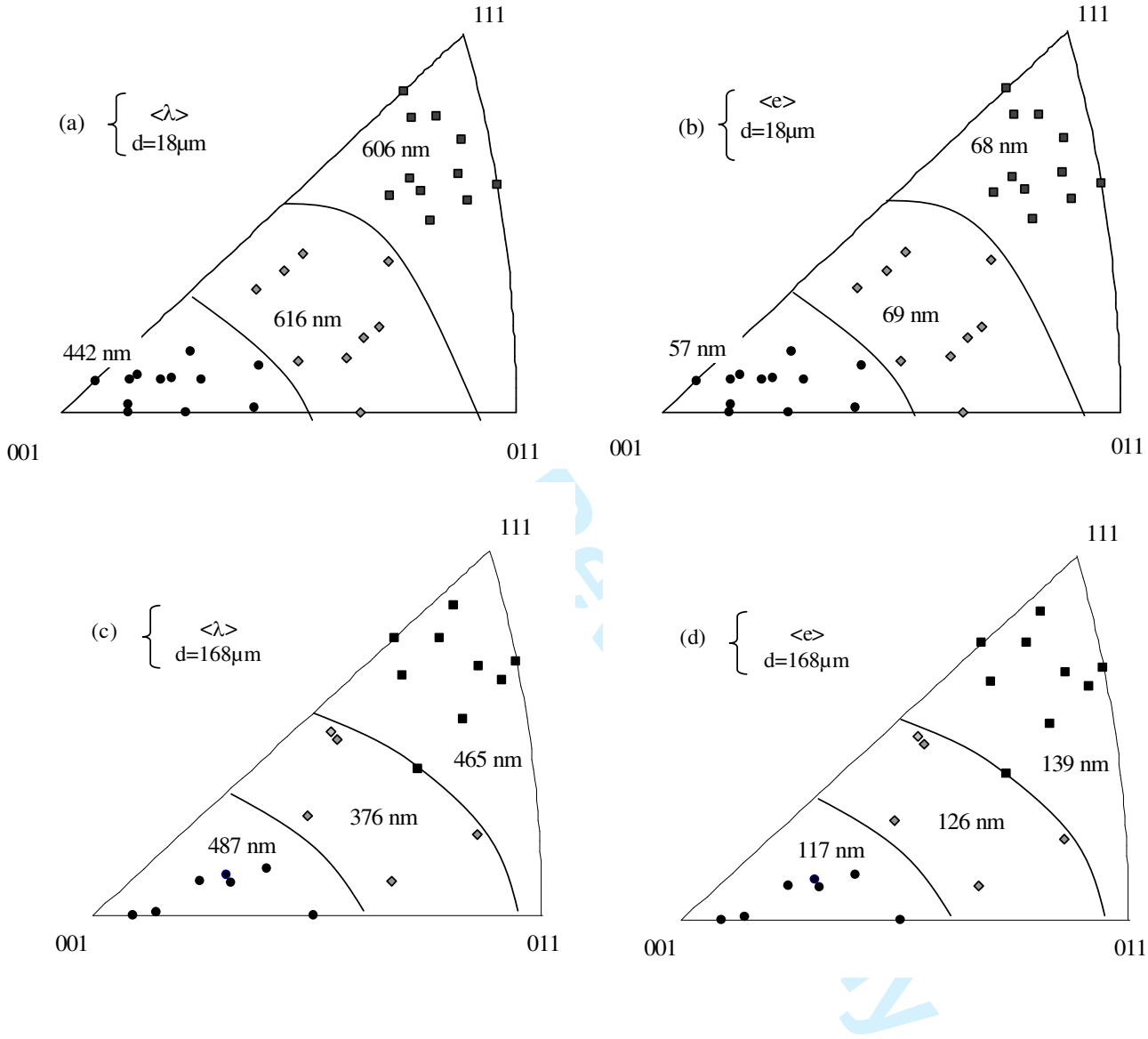


Figure 12: Definition of three orientation fields on inverse pole figure in term of IDB spacing (a, c) and IDB thickness (b, d) for two grain size (18 μm (a, b) and 168 μm (c, d) in nickel.

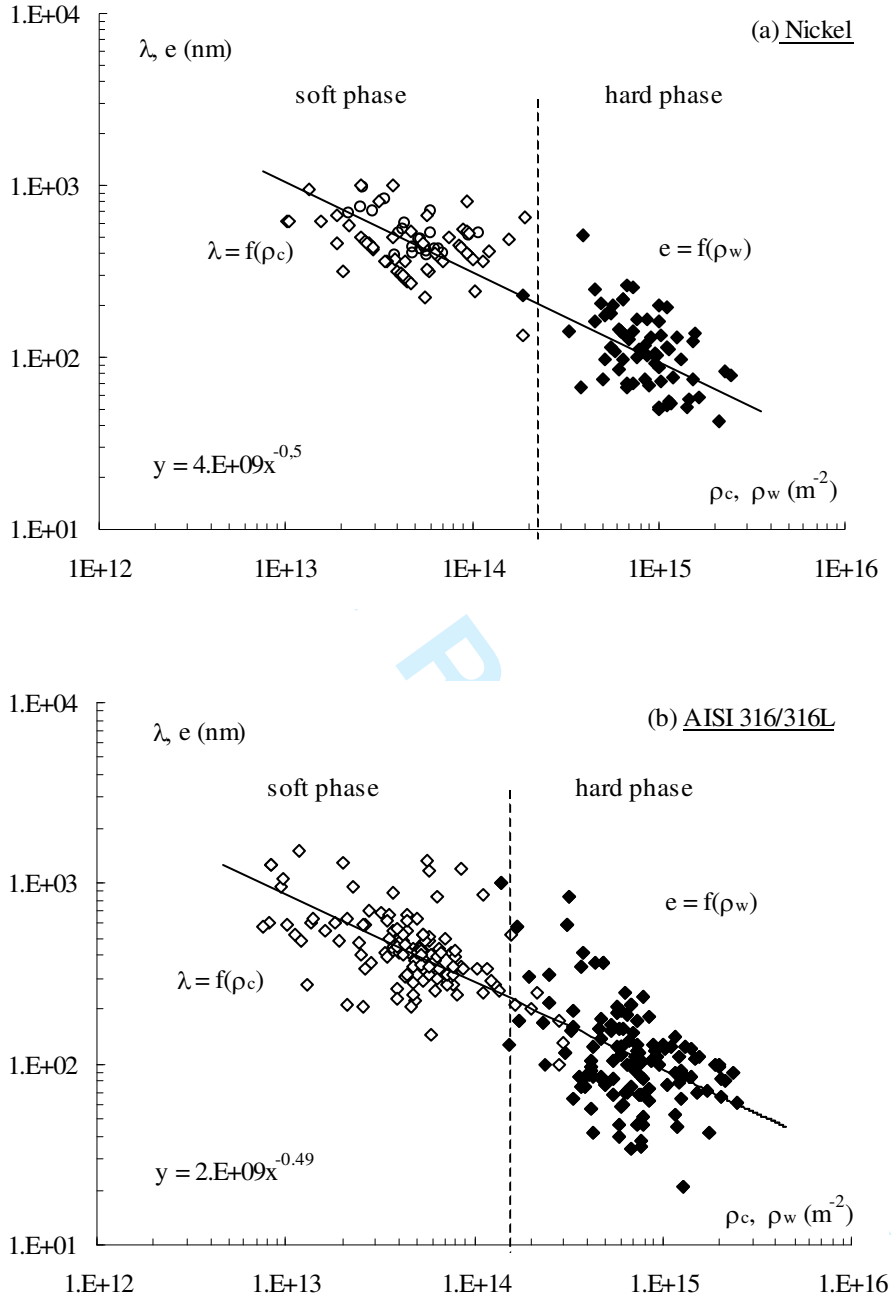


Figure 13: Correlation between thickness e and spacing λ and respectively the density of dislocation in wall $\rho_w$ and in inter-wall spacing $\rho_c$. (a) in nickel each point corresponds to one grain observed in Ni-D (168µm) or in Ni-A (18 µm) after a tensile strengthening ($\varepsilon_p$=0.3). (b) in AISI 316/316L each point corresponds to one grain observed after tensile strengthening (stages II and III) [40, 62], cyclic loading under strain control [43, 45] and stress control [43, 48] (stages $II_0$, $III_0$, III).

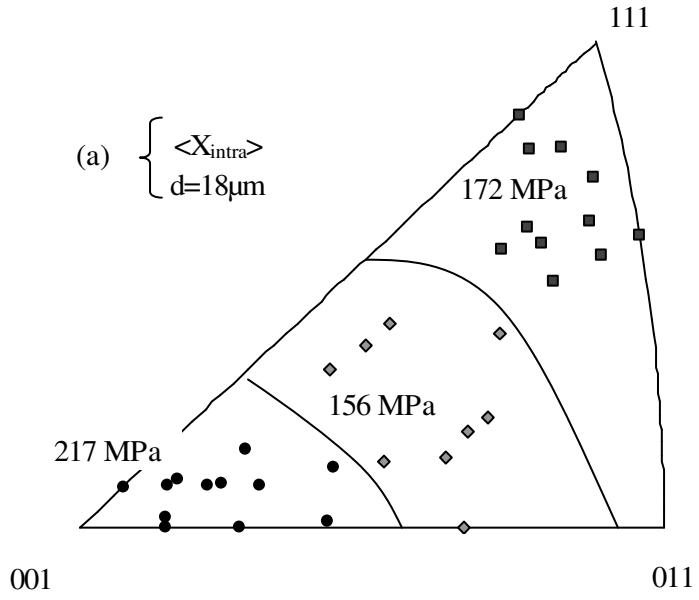


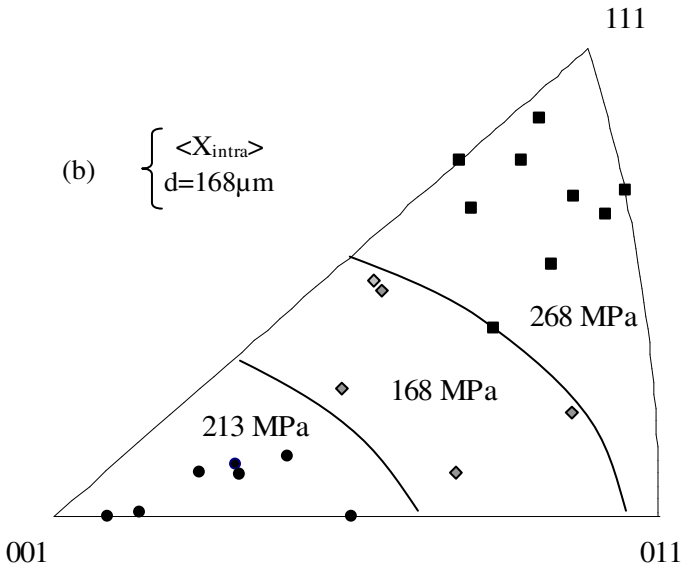


Figure 14 : Definition of three orientation fields on inverse pole figure in term of intra-granular long-range internal stresses $<X_{intra}>$ for two grain size in nickel: 18 µm (a) and 168 µm (b).

| Metal | Nickel (d = 18 µm) | Nickel (d = 168 µm) | 316 L (d = 53 µm) |
|---|---|---|---|
| $X_{intra}$ (comp. modelling) | 185 MPa | 245 (MPa) | 418 (MPa) |
| $X_{intra}$ (Hall-Petch) | 240 (MPa) | 240 (MPa) | 405 (MPa) |

Table 1: Comparison between intra-granular long-range internal stresses $\overline{X}_{int\,ra}$ obtained using composite modelling and Hall-Petch approach [28, 30].